Coordinates

THE MONTHLY MAGAZINE ON POSITIONING, NAVIGATION AND BEYOND

Volume XIX, Issue 8, August 2023

Performance assessment of GAGAN for aircraft precision approach

Distributed GNSS Positioning-as-a-Service: Death of a Traditional GNSS Receiver?
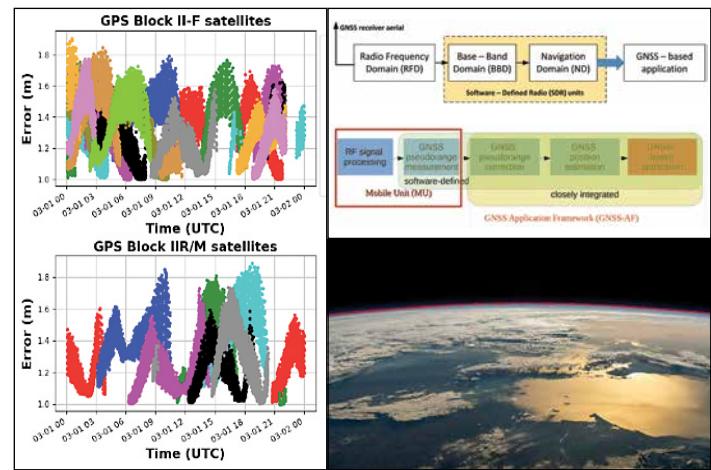
SAVE THE DATE

INTERGEO®

OCT. 10-12 **2023**

BERLIN

#INTERGEO

DVW

WWW.INTERGEO.DE

In this issue

Coordinates Volume 19, Issue 8, August 2023

GAGAN – In aviation and beyond

The GPS-aided GEO augmented navigation (GAGAN) -

The Indian satellite based augmentation system (SBAS),

Has widely been used in aviation since its inception.

However, the applications in non-aviation segments

Such as railways, surveys, marine, disaster management, LBS, research …

Have been not only been encouraged but also publicised time to time

Like Real Time Train Information System, Gagan
Message Service (GAMES) and many more.

As in this issue of Coordinates, Mr Narayan Dhital provides

An assessment of GAGAN performances for precision
aircraft approach and landing (page number 9),

Would n't it be prudent to evaluate if the potential of GAGAN
applications in other segments has been optimized?

Bal Krishna, Editor
bal@mycoordinates.org

Distributed GNSS positioning-as-a-Service: Death of a traditional GNSS receiver?

A traditional perception of a black-box GNSS receiver served for the GNSS PNT has dramatically evolved into a completely novel concept of distributed GNSS Positioning-as-a-Service, utilising the latest developments in computer science, mathematics, and statistics

Renato Filjar

Electrical engineer, a Titular Professor of Electronics Engineering (Tenure) with Faculty of Engineering, University of Rijeka, Rijeka, Croatia, and a Professor of Electrical Engineering & Head of Laboratory for Spatial Intelligence, Hrvatsko Zagorje Krapina University of Applied Sciences, Krapina, Croatia.

Filip Šklebar

Electrical engineer, and an external associate to Laboratory for Spatial Intelligence, Hrvatsko Zagorje Krapina University of Applied Sciences, Krapina, Croatia

Ivica Zubić

Traffic Engineer, and a Lecturer with Laboratory for Spatial Intelligence, Hrvatsko Zagorje Krapina University of Applied Sciences, Krapina, Croatia.

A traditional perception of a black-box GNSS receiver served for the GNSS PNT has dramatically evolved into a completely novel concept of distributed GNSS Positioning-as-a-Service, utilising the latest developments in computer science, mathematics, and statistics.

Satellite navigation has become an essential cornerstone of modern civilisation, a fundamental component of national infrastructure, and a public goods, enabling and driving a vast range of technology, and socio-economic systems and services. A prevalent view of GNSS utilisation still depicts an image of a user with a device in his or her hand magically producing position and velocity estimates and perfect timing synchronisation using some marvels of mathematics and statistics, signal processing, radio communications, electrical and mechanical engineering. While such an image may be found in diminishing number of occasions, such a description of GNSS Positioning, Navigation, and Timing (PNT) service is not only changing, but has become obsolete. Recent developments in computer science, mathematics and statistics, and signal processing have revolutionised a traditional view of a black-box GNSS receiver performing the complete GNSS position estimation process [10]. Introduction of the Software-Defined Radio (SDR) concept, Machine Learning (ML) methods and algorithms, fast internet connections and

advanced computational techniques, such as Cloud Computing, renders the GNSS position estimation process more resilient to external (environmental) adversarial and detrimental effects, distributed and, therefore, transparent [6, 7, 10]. Transparency and resiliency of GNSS position estimation process has opened an enormous room for developments, enhancements, and improvements which leads to en entirely new concept of GNSS Positioning-as-a-Service, described in this manuscript. The GNSS Positioning-as-a-Service concept is defined as a mathematics-established and software-based GNSS position estimation process set on a distributed computing platform.

The traditional concept of GNSS positioning has equalised the GNSS position estimation process with a GNSS receivers, rendering it a black-box delivering position, velocity, and time estimates [7, 10]. Such a concept was suitable for initially anticipated military applications of satellite navigation. It was later transferred into commercial domain through the process of wider acceptance of satellite navigation [1, 7].

The GNSS PNT service is conducted through the GNSS position estimation process, comprising three essential domains [3, 5, 6, 7], as depicted in Figure 1: (i) Radio Frequency Domain (RFD), (ii) Base-Band Domain (BBD), and (iii) Navigation, or Application, Domain (ND).

In the reference to GNSS positioning tasks, the RFD deals with the received modulated satellite signals performing conditioning, demodulation, and conversation of the signals. The BBD measures raw GNSS pseudoranges and extracts related information from the Navigation Message. The ND applies detrimental effects counter measures on raw GNSS pseudorange measurements, such as the ionospheric and tropospheric delays corrections, and performs the GNSS position and positioning errors estimation based on the Navigation Message information and the mitigated GNSS pseudoranges. Selection and applications of methods and techniques for the GNSS position estimation process are governed by the characteristics of the system architecture selected for the GNSS position estimation process implementation [6, 7].

Traditional concept of a GNSS receiver assumes the prevalent utilisation of dedicated electronic circuits, electrically pre-programmed to perform a dedicated tasks. The concept allows for fitting into a single black-box GNSS receiver unit, but lacks flexibility in modification, upgrade, and multi-usage of the initially pre-defined hardware of a particular purpose [6, 7].In the process of increased utilisation of GNSS as the critical and enabling foundation technology, the traditional view on the user equipment, GNSS receivers, has started to emerge as

a growing obstacle to development. As it happens with every technology, satellite navigation is vulnerable to numerous adversarial effects, both natural, such as space weather/ionospheric and multipath causes of satellite signal delays and reception disruptions, and artificial, such as spoofing, meaconing, and jamming [2, 4, 5, 6, 8, 12, 13]. GNSS operators attempt to assist with mitigation of such effects using the globalised correction models, augmentation systems such as EGNOS and WAAS, and the provision of additional information for the internet-connected user equipment. The attempts generally yield a mixed success, as majority of the effects are related to GNSS positioning environment conditions in the immediate vicinity of the unknown position at which the GNSS signal reception takes place [7]. The GNSS operator is prevented in the provision of the suitable correction and mitigation information by the very nature of the GNSS position estimation and the inability to be aware of the user's GNSS positioning environment at a required scale. Furthermore, the results of the GNSS positioning process serve increasingly a GNSS application, system or a service, and are generally not presented in its raw form to the GNSS end-user [6, 7]. The manner of assessment of the GNSS positioning performance is more related to the core GNSS processes, and, consequently, suits the traditional view of a GNSS receiver. However, it fails in establishing a productive and

pragmatic compliance with the needs and requirements of a GNSS application that will utilise GNSS position estimates to produce a service or an information based on GNSS-based position estimate. GNSS applications need some form of GNSS positioning error estimate to determine the Quality of Service (QoS) of a particular GNSS application [1, 7, 10]. For instance, GNSS operators usually express the estimated positioning error in terms of ideal positioning environment conditions: unobstructed view of horizon, averaged ionospheric and multipath effects. The approach yields the range of GNSS positioning errors, in anticipated extremes, which are generally of sparse use for GNSS application developers, operators, and users, since the positioning error estimates may fluctuate over time widely and unexpectedly in and out of the acceptable range for the particular GNSS application.

The shortcomings of the traditional approach in implementation of the GNSS positioning process through a single black-box mobile GNSS receiver may be summarised as follows: (i) GNSS pseudorange error correction using the global models fail in recognition of the real positioning environment conditions, which render them sub-optimal and generally inefficient in the mitigation of various adversarial effects on GNSS PNT. (ii) Specification of the core GNSS PNT QoS do not translate into GNSS-based application QoS needs, which reduces and limits significantly potentials for GNSS application development and operation. (iii) GNSS augmentation and assistance, such as SBAS: WAAS, EGNOS require additional infrastructure, which is generally very complex and expensive for establishment, operation, and maintenance and still provide sub-optimal results in mitigation of the adversarial effects on GNSS PNT. (iv) The raising number of artificial adversarial effects on GNSS performance and operation requires additional infrastructure and effort for mitigation of their causes (GNSS spoofing, jamming, and meaconing) [2], as GNSS cyberattacks which may additionally raise the mitigation costs.
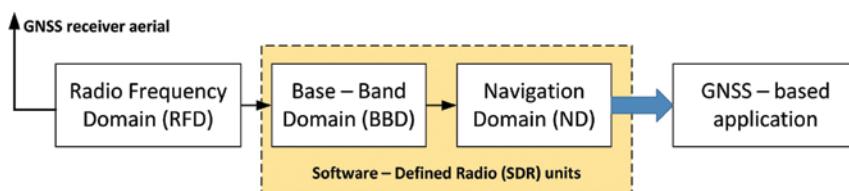

Figure 1. GNSS position estimation process is extended over three essential domains, two of them now implemented as a software-based platform of the Software-Defined Radio, SDR.
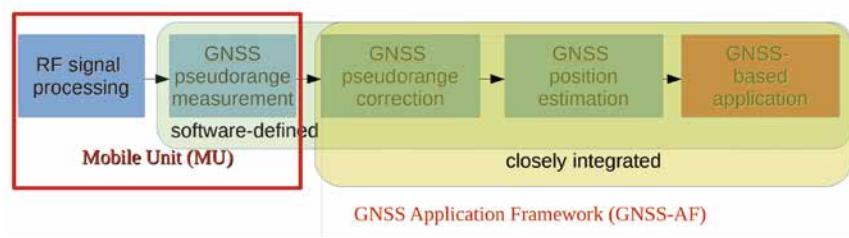

Figure 2. Distributed GNSS Positioning-as-aService

Our international research team assessed the recent related developments, including: (i) Software-Defined Radio concept utilisation in user segment of GNSS that renders the GNSS positioning process transparent and manageable, (ii) abundance of machine learning methods and techniques, suitable for a wide range of classification and regression (predictive modelling) problems solving, (iii) breakthrough developments in the provision of fast, reliable, and ubiquitous mobile internet communications, (iv) available and affordable advanced computing frameworks and methods, such as cloud computing, (v) availability of machine-readable positioning environment-related data, such as space weather and ionospheric conditions observations, (vi) structured classification of GNSS applications and their needs and requirements for GNSS PNT performance. The assessment results in the proposal of a novel concept in definition, description, and deployment of GNSS positioning process, we called the GNSS Positioning-as-a-Service [7]. The new concept is depicted in Figure 2.

The GNSS Positioning-as-a-Service extend the architecture comprising a *Mobile Unit (MU)* and a *GNSS application Framework (GNSS-F)*, connected via mobile internet service [7]. The GNSS positioning process is distributed here between the two constitutional units. The MU performs tasks related to the initial RF signal processing and the Base-Band Domain (GNSS pseudorange measurement and extraction of related data from Navigation Message), and packs the tasks results (raw GNSS pseudorange measurements observed Navigation Message data, and optional observations of the immediate GNSS positioning environment conditions, such as geomagnetic field density components values, if the MU is equipped with the suitable sensors) into a tailored protocol for transmission to cloud-based unit. The GNSS-AF utilises the observations of the immediate GNSS positioning environment conditions, if received, and trusted third-parties observations and estimations for development and operation of bespoke

The proposed GNSS Positioning-as-a-Service emerges as a groundbreaking novelty, providing numerous benefits and advantages, while opening widely the room for robust and QoS-guaranteed GNSS applications development and operations

machine learning-based correction models for mitigation the adversarial effects contained in raw GNSS pseudoranges [5, 6, 7, 9]. GNSS pseudoranges become corrected optimally in the sense of the actual immediate GNSS positioning environment conditions. Corrected GNSS pseudoranges then serve as inputs to GNSS position estimation algorithm, which software implementation returns the improved position estimates. In that sense, the cloud-based unit performs the tasks of the Navigation Domain of the GNSS positioning process.

The proposed GNSS Positioning-as-a-Service concept recognises a GNSS application closely integrated with the task related to Navigation within the GNSS-AF. This novelty establishes a GNSS application in charge of definition, development and operation of correction models, as well as of selection of the position estimation methods, all of them in relation to the needs and requirements for the GNSS PNT performance for the GNSS application in question. The integration between the Navigation Domain tasks and a GNSS application anticipated to use the results of the GNSS positioning process resolves the lack of compliance with the core GNSS positioning performance and the needs and requirements for the GNSS application QoS [1, 7]. As the result, the GNSS position estimates emerge as optimised to the PNT needs and requirements of a GNSS application [7].

The active involvement of a GNSS application in the GNSS positioning process allows for tailored configuration of GNSS positioning performance as optimised to the needs and requirements of GNSS application. It utilises the

situation awareness concept of mitigation the adversarial effects on GNSS PNT in consideration of the actual positioning environments conditions, based either on the mobile unit's observations, or on data provide by trusted third-party providers (US NOAA, US NASA, EU Copernicus etc.) [5, 7, 9, 10]. The proposed GNSS Positioning-as-a-Service allows for re-definition of the GNSS positioning performance, including accuracy, in terms of scenarios and conditions of actual utilisation. This approach relieves the GNSS operators of the mission-impossible task to guarantee the GNSS PNT performance, determined mostly with the users positioning micro-environment conditions, the scenario of usage, and the meeds and requirements of a GNSS applications which are all unknown to the GNSS operator. Within the GNSS Positioning-as-a-Service concept, the GNSS operator may focus on advanced spectrum management and protection, and signal structure improvement and protection, without the involvement in issues outside its outreach and control.

Our research team has developed a laboratory GNSS Positioning-as-a-Service development and simulation framework, based on the software developed in the open-source R environment for statistical computing. The framework operates in Laboratory for spatial Intelligence of Hrvatsko Zagorje Krapina University of Applied Sciences in Krapina, Croatia. It serves research in mathematics, statistics, signal processing, and computer science in relation to advance the GNSS PNT performance with the novel position estimation methods, and for detection, identification and mitigation of both natural and artificial adversarial effects

on GNSS PNT performance. The results accomplished make contribution to scientific developments, while at the same time being exploiting in industry, and serving as important source of knowledge in the academic education process.

The proposed GNSS Positioning-as-a-Service emerges as a groundbreaking novelty, providing numerous benefits and advantages, while opening widely the room for robust and QoS-guaranteed GNSS applications development and operations. Enhanced PNT performance, detection of and resilience against natural and artificial (spoofing) [2] adversarial effects on GNSS PNT, alignments to GNSS application QoS, and quantifying the risk of the GNSS uitilisation for particular GNSS-based application [11, 12] are among the numerous opportunities resulting from the GNSS Positioning-as-a-Service implementation and operation. The novelty also opens a number of challenges to the existing framework of the GNSS PNT performance management, as GNSS positioning enters the field of ICT services, including: redefinitions of regulations and processes, operations, standardisation & certification, regulations of operations and international trade, international co-operation, targeted academic and professional education. While our team continuous in research, development and exploitation of the proposed concept, we believe the GNSS Positioning-as-a-Service is to set the new standard, attract research interest, and open the vast range of developments, advancements, and co-operation in the field of satellite navigation and its applications.

Reference

[1] EUSPA. (2023). User Consultation Platform (UCP) User Needs and Requirements 2022 (Library contains Reports on: (1) Aviation and Drones, (2) Consumer Solutions, (3) Emergency Management and Humanitarian Aid, (4) Energy and Raw Materials, (5) Infrastructure, (6) Insurance and Finance, (7) Maritime, Inland Waterways, Fisheries and Aquaculture). European Agency for Space Programme (EUSPA). Prague, Czechia. Available at: https://www.euspa.europa.eu/ucp-user-needs-requirements-2022

[2] Filić, M. (2018). Foundations of GNSS Spoofing Detection and Mitigation with Distributed GNSS SDR Receiver. TransNav, 12(4), 649-656. doi: http://dx.doi.org/10.12716/1001.12.04.01

[3] Filić, M, Filjar, R. (2018a). Smartphone GNSS positioning performance improvements through utilisation of Google Location API. Proc of 41 st International Convention MIPRO/CTI, 507-510. Opatija, Croatia. doi: https://doi.org/10.23919/MIPRO.2018.8400087

[4] Filić, M, Filjar, R. (2018b). A South Pacific Cyclone-Caused GPS Positioning Error and Its Effects on Remote Island Communities. TransNav, 12(4), 663-670. doi: http://dx.doi.org/10.12716/1001.12.04.03

[5] Filić, M, Filjar, R. (2018c). Modelling the Relation between GNSS Positioning Performance Degradation, and Space Weather and Ionospheric Conditions using RReliefF Features Selection. Proc of 31st International Technical Meeting ION GNSS+ 2018, 1999-2006. Miami, FL. doi: https://doi.org/10.33012/2018.16016

[6] Filić, M, Grubišić, L, Filjar, R. (2018). Improvement of standard GPS position estimation algorithm through utilization of Weighted Least-Square approach. Proc of 11th Annual Baška GNSS Conference, 7-19. Baška, Krk Island, Croatia. Available at: https://www.pfri.uniri.hr/web/hr/dokumenti/zbornici-gnss/2018-GNSS-11.pdf

[7] Filjar, R. (2022a). An application-centred resilient GNSS position estimation algorithm based on positioning environment conditions awareness. Proc ION ITM 2022, 1123 - 1136. Long Beach, CA. doi: https://doi.org/10.33012/2022.18247

[8] Filjar, R. (2022b). A contribution to short-term rapidly developing geomagnetic storm classification for GNSS ionospheric effects mitigation model development. ICEASE 2021 Conference. Islamabad, Pakistan. doi: https://doi.org/10.1109/ICASE54940.2021.9904168

[9] Filjar, R, Weintrit, A, Iliev, T, Malčić, G, Jukić, O, Sikirica, N. (2020). Predictive Model of Total Electron Content during Moderately Disturbed Geomagnetic Conditions for GNSS Positioning Performance Improvement. Proc USION2020, 256-262. Pretoria, South Africa. doi: https://doi.org/10.23919/FUSION45008.2020.9190264

[10] Filjar, R, Damas, M C, Iliev, T B. (2020). Resilient Satellite Navigation Empowers Modern Science, Economy, and Society. CIEES 2020. IOP Conf. Ser: Mater Sci Eng 1032, 012001 (10 pages). Borovets, Bulgaria. doi: 10.1088/1757-899X/1032/1/012001

[11] Malić, E, Sikirica, N, Špoljar, D, Filjar, R. (2023). A method and a model for risk assessment of GNSS utilisation with a proof-of-principle demonstration for polar GNSS maritime applications. TransNav, 17(1), 43-50. doi: http://dx.doi.org/10.12716/1001.17.01.03

[12] Sikirica, N, Dimc, F, Jukić, O, Iliev, T B, Špoljar, D, Filjar, R. (2021). A Risk Assessment of Geomagnetic Conditions Impact on GPS Positioning Accuracy Degradation in Tropical Regions Using Dst Index. Proc ION ITM 2021, 606-615. San Diego, CA. doi: https://doi.org/10.33012/2021.17852

[13] Špoljar, D, Jukić, O, Sikirica, N, Lenac, K, Filjar, R. (2021). Modelling GPS Positioning Performance in Northwest Passage during Extreme Space Weather Conditions. TransNav, 15(1), 165-169. doi: http://dx.doi.org/10.12716/1001.15.01.16

GAGAN performance assessment for aircraft precision approach

The study provides an assessment of GAGAN services for APV–I and APV–II over the Indian territory. Satellite error bounds and ionospheric error bounds are analyzed as the main contributing integrity parameters.

Narayan Dhital

Actively involved to support international collaboration in GNSS-related activities. He has mainly supported and contributed to different workshops of the International Committee on GNSS (ICG), and the United Nations Office for Outer Space Affairs (UNOOSA). As a professional employee, the author is working at the Galileo Control Center, DLR GfR mbH, Germany

Abstract

This article provides an assessment of GAGAN performances for precision aircraft approach and landing. The single-frequency GPS-based SBAS requirements set by ICAO are used to assess the GAGAN satellite integrity messages and compared against other existing global SBAS systems. It is evident from the analysis that GAGAN is capable to support RNP 0.1 aircraft procedures and for most of the period also the APV-I procedures. But the 99.99% availability is not met for APV-I and APV-II is a bit far-fetched. The impact of the ionospheric events is larger for the GAGAN system than the established WAAS and EGNOS. For the characterization of the observed performances, three critical points are focused on throughout the article: a. zero-mean Gaussian assumption of the integrity system b. correction confidence bound for satellite clock and orbit, and c. ionospheric model and threat space. An insight into the potential evolutions of the integrity systems and the performances are given considering two aspects: a. Dual-Frequency Multi-Constellation b. consideration of individual bias to accommodate non-zero mean and non-Guassian measurement errors rather than conservative inflation of the variances. The findings from the article attempt to bridge the gap in the literature regarding the GAGAN system integrity performances.

Introduction

GPS Aided Augmentation System (GAGAN) is one of the latest SBAS systems certified for en-route aircraft operation since 2013 (**PBI, 2015**). As the first system in the equatorial region, GAGAN System was certified by DGCA in 2015 for Approach with Vertical Guidance (APV 1) and en-route (RNP 0.1) operations. In recent years, there have been successful trials and implementation of GAGAN-based aircraft procedures in Indian airports). There is also a mandate by DGCA for all new aircraft after 2021 to be GAGAN-equipped (**PBI, 2022**). On top of that the recent public information regarding the order of a large number of aircraft fleets from Airbus and Beoing is a testament to a flourishing downstream market for the GAGAN system (**Indiantimes, 2023**). The technical description of the system and application is provided in the GAGAN information portal and its literature section (**AAI, 2023**). From a technical perspective, the integrity system is similar to the existing EGNOS and WAAS and adheres to the ICAO MOPS (**AAI, 2023**). However, the literature on the performance evaluation of the GAGAN system is very limited (**Insidegnss, 2016**). There is couple of analysis from Thailand and Srilanka (**Sophan, 2022**) but only focused on the user positioning accuracy.

Regarding the necessity of the integrity performance assessment, it has been well known that it is not possible to compute the actual error introduced by satellites in real-time flight operations. At the same time, the errors introduced by the user aircraft, mostly the noise and multipath, are not known to the SBAS integrity monitoring system. The only way possible for integrity provision is to bound in real-time the potential user error in the worst-case scenario and

protect the user from hazardously misleading information. This has to be validated by the data analysis based on the established model. It has been a common concept since the early days of the SBAS integrity system to consider the zero-mean Gaussian nature of measurement errors that are observed in the system monitoring side. The total variance of error terms can be computed by a simple summation of each error term as all errors are independent and uncorrelated. These simple assumptions allow the propagation of covariance from psuedorange domain to the position domain and obtain the protection level (**Walter et. al, 1999, NAVIPEDIA, 2006, Ober et .al, 2023**).

Figure 1 represents the Gaussian distribution of the actual errors fully defined by the variance term and the mean value and the overbounding Gaussian distribution defined by only the variance term. It is the overbounding gaussian distribution that is broadcast to the user as the integrity parameter. The inflation of the Gaussian distribution is activated when the threshold is reached by the bias in the measurement error. The bias caused by the faulty situation could still be well below the threshold and covered by the tail of the zero-mean nominal gaussian distribution. The K- factor makes sure that only the allowed probability of missed detection of bias and faults occurs. When the bias is just above the threshold, the Gaussian distribution is inflated but the zero-mean property is still conserved. In this way, the overbound distribution covers the tail error probability as well as the peak error probability. The K number is computed as the minimum value for the given σ_0 (and $> \sigma_a$). This creates an overbounding Gaussian distribution which is tangent at the point to the actual distribution and above it at all other points. To also consider the individual bias μ_a, it is best to optimize σ_0 and K factor that minimizes the protection level.

$$K\, N_y\,(\mu_o, \sigma_0)\ \geq\ N_y\,(\mu_a, \sigma_a) \tag{1}$$

$$\frac{K}{\sigma_0}\, e^{-\frac{y^2}{2\sigma_0^2}} \geq \frac{K}{\sigma_a}\, e^{-\frac{(y-\mu_a)^2}{2\sigma_a^2}} \tag{2}$$

Here the K value depends on the tolerable probability of having an error greater than the protection level value. For a probability the K value is 5.33. The derivation of the K value is well documented in the references (**RTCA, 2020, NAVIPEDIA, 2006**). It is computed from the basic statistical law of the cumulative distributive.

K (V_PA) = Normal $cdf^{-1}(1-\frac{10^{-7}}{2}) = 5.33$, for one-sided exceed probability of $\frac{10^{-7}}{2}$

K (H_PA) = Normal $cdf^{-1}(1-\frac{10^{-9}}{2}) = 6.0$, for one-sided exceed probability of $\frac{10^{-9}}{2}$

The zero-mean Gaussian assumption is key because it overbounds the nominal (fault-free) errors in the measurements. The individual error (residual variance) is independent and uncorrelated and hence the total variance per satellite is also Gaussian in nature. This also has an implication in the system monitoring where statistical analysis such as the Chi-square test

can be used to detect and remove bad data as the summation of multiple Gaussian distributions follows the Chi-Square distribution. In such a distribution, the K factor inflates the variance to consider the probabilities of error occurrence in the tail of the Gaussian distribution. This same approach and assumption in the system side of the SBAS and the user aircraft allow to compute the integrity. There is no reliable way to know the actual errors in real-time at any location and there could be a bias coming from the user location which is violating the Gaussian distribution, in that case, it would be a hazardous situation if position error is indeed above the protection level and the alert limit. Though, it needs to be recalled that even in the nominal situation the error distribution does not follow the perfect Gaussian distribution (as explained in Figure 1). The only way to provide integrity is to overbound it using the Gaussian distribution with inflated variance. When propagated in the position domain, the PL is increased to protect the user. It is also difficult to inflate the PL for all scenarios in real-time and the incorporation of biases originating in fault scenarios is not straightforward. (**Insidegnss, 2020**) shows in an intuitive statistical simulation why and how Gaussian distribution is assumed and how inflated distribution protects the user. The bias coming from Satellites is well observed by the RIMS. The correction confidence bound (covariance matrix) helps to lower the variance based on the location of users. Only the ionospheric events are tricky to handle where the specific bias could arise to some users which are not captured by the observations in the RIMS Iono model. But to some extent, this factor is also considered in
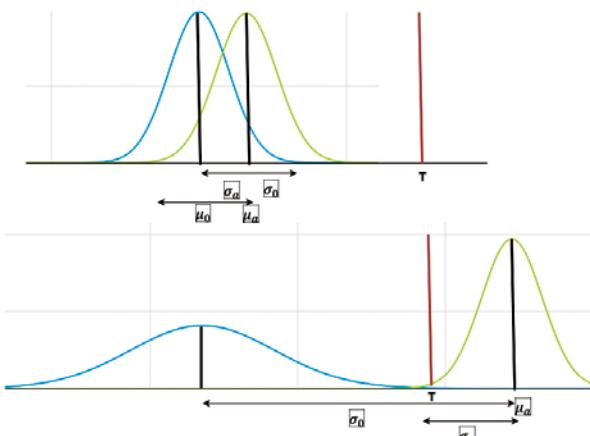
Figure 1: (Top) The nominal distribution of the GAGAN measurement errors shown in the blue curve with . It overbounds the actual distribution of the error represented by the yellow curve with. The biased distribution is well within the threshold indicated by red line. In this scenario, the nominal distribution protects the user without inflating the variance. **(Bottom)** The biased distribution is just above the defined threshold. In this scenario the GAGAN system shall treat it as a fault like scenario. The broadcast integrity information can still accommodate the fat tail–error distribution as it broadcast the inflated variance based on the zero–mean Gaussian distribution shown by the blue curve. Without a need to consider the bias in faulted scenario, the inflated variance overbounds the tail of the true error distribution. The 1–sigma value is scaled by the K factor, which is determined as in Equation 1 and 2.

the GIVE computation. The only drawback with these is that the variance is inflated for all users to protect from any threat and hence the availability is impacted. Such conservative assumptions have multiple limitations: a. the actual correlations appear to be negative b. they combine to reduce the overall positioning error rather than increase it (**Walter et. al, 1999**).

Is there a way to consider the integrity on the user side where the biases are also considered without having to inflate the variance? Some insights into it will be provided later in this paper.

In terms of mathematical formulation, the following equations (Equations 3-8) capture the essence of individual errors characterized by independent, zero-mean normal distributions, and the global residual pseudo-range error for each satellite (i-th ranging source) that may also be characterized by the zero mean normal distribution whose variance is simply expressed as the summation (Equation 4).

$$PL = k_{V/H} \sqrt{\sum_{i=1}^{N} S_i^2 \, \sigma_i^2} \quad (3)$$

$$\sigma_i^2 = \sigma_{i,flt}^2 + \sigma_{i,UIRE}^2 + \sigma_{i,a/c}^2 + \sigma_{i,Tropo}^2 \qquad (4)$$

$$\sigma_{i,flt}^2 \propto I^T P I \qquad (5)$$

$$\Delta \hat{x} = (G^T W G)^{-1} G^T W \Delta \hat{y} \qquad (6)$$

$$P = (G^T W G)^{-1} \qquad (7)$$

$$P = \begin{bmatrix} d_E^2 & d_{EN} & d_{EU} & d_{ET} \\ d_{EN} & d_N^2 & d_{NU} & d_{NT} \\ d_{EU} & d_{NU} & d_U^2 & d_{UT} \\ d_{ET} & d_{NT} & d_{UT} & d_T^2 \end{bmatrix} \qquad (8)$$

here P gives the full covariance matrix which is available in the position solution computation.

The right side of equation 3 is in fact the third diagonal element from this covariance matrix. The S term is the partial derivative of the error in vertical direction w.r.t the pseudorange error for the ith satellite. The weight matrix W is the inverse of the variance for each satellite broadcast in the integrity message.

Impacts of satellite orbits and clocks on GAGAN

Each existing SBAS has its threat model for satellite orbits and clocks to generate corrections and confidence-bound information meeting integrity requirements. Each threat model should fit its service area. The range error due to the fault on board the satellite clocks can be observed from all ground stations simultaneously and thus detected easily. For the satellite orbit error, a non-nominal condition is not likely as the GNSS satellites follow the orbit dynamics. The exceptional case of

orbit delta V maneuver and attitude maneuver is also predicted and detected by the network of the ground station. The pseudo-dynamic orbit prediction which uses both the deterministic approach based on the physics and the measurement data provides better confidence in the orbit position. To some extent, the satellite clock estimation is stochastic as the clock offset is characterized by a random walk process. Regardless of it, the anomaly in the satellite clock can be detected by all ground stations. In the nominal scenario, the most important consideration for satellite ephemeris is needed regarding the service coverage zone. The Message Type 28 Covariance Matrix provides the confidence weight for each satellite based on the user location. Equation 5 shows the relationship between the modified variance of the satellite corrections using the information from MT 28. It allows the lower inflation of the variance for the satellite which has been well-monitored (through good geometry) in the system. The confidence bound for GPS satellite orbit and clock correction is location dependent, where I is the line of sight from satellite to user aircraft, P is the covariance matrix derived from the same estimation procedures that compute the range error of the satellite clock and orbit (often called User Differential Range Error (UDRE)).

To experimentally test this, the covariance matrix from MT28 is used to compute the delta User Differential Range Error (UDRE), which is dependent on the location of the airspace from where the aircraft will receive the satellite signals. The confidence interval of each satellite orbit and clock error on the line of sight is multiplied with the broadcast UDRE to get the final variance in the protection level calculation. The better the location of the aircraft w.r.t the observability of GPS satellites monitored by the GAGAN network, the better the protection level. An example analysis using the Kazakstan airspace (within the GAGAN Geo footprint) is shown in the results and interpretation chapter.

Impacts of Ionospheric events on GAGAN

Non-nominal ionospheric events make the largest threat to aircraft procedures. Each existing SBAS has its ionosphere threat model to generate ionospheric correction information meeting integrity requirements. Each threat model should fit its service area. As ionospheric activity is a dynamic and natural phenomenon, none of the threat models assure overbound anomalous events forever (**ICAO, 2016**). Regular ionospheric monitoring is therefore essential to confirm that the threat space is overbounding the anomalies. For the GAGAN system, the distribution of the monitoring network is not robust enough to capture anomalies in the coverage edge (**Sophan, et. al, 2020**). On top of that the coverage zone consists of a highly active equatorial ionospheric zone. Scintillation effects are also prominent and impact the received power and phase of GNSS signals and as such can cause loss of lock on the GNSS signals and render the unavailability and discontinuity of the system. The ionosphere threat model is the actual function representing the associated threat space

which has to cover the existence of the largest ionospheric irregularities that might not have been sampled in the system ground station (**Sparks, et. al, 2021, ICAO, 2016**). This is depicted in Figure 2. In the next section, a detailed analysis is performed to examine the GAGAN performances during the nominal ionospheric situation and active geomagnetic storm days.

Analysis data set and methods

The selected timeframe for the analysis is summarized in **Table 1**.

The GAGAN messages are retrieved from CNES ftp server. For the user observation of GPS satellites, the RINEX files from UNAVCO and CDDIS ftp servers are used. The user observation of GPS data are collected from different GNSS stations as indicated in **Table 1**. The site name "KTM" refers to the station data from Kathmandu, Nepalese airspace. Similarly "KZT" referes to Kazakhstan.
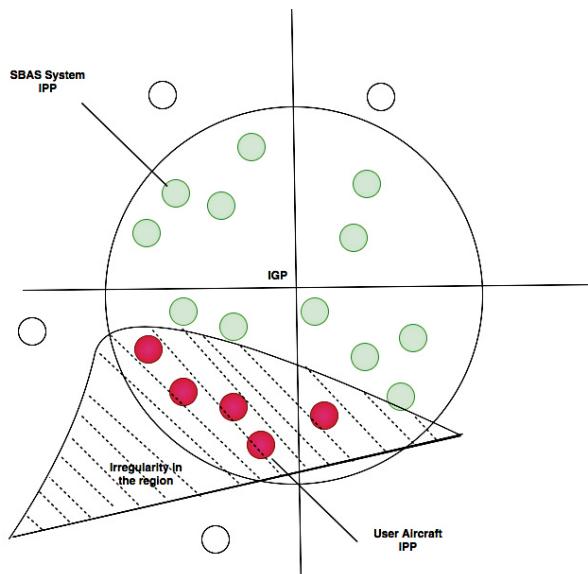
Figure 2: The ionospheric model is based on the grid point radius where the system observes the ionospheric anomalies from various ionospheric pierce points. In the absence of a monitoring station in the region where users are using the service, the irregularities could go unobserved by the model and hence the variance term could be either largely inflated or fixed to the values derived from the nearest IGPs. This renders increased protection levels and potential service unavailability. In some cases, the protection level might not capture strong irregularities and hence actual error could be higher than the protection level and alert limits without inflating the protection level. This renders hazardously misleading information.

As the current solar cycle 25 is approaching its maximum, there are frequent opportunities to analyze the impact on the performance of the GAGAN system. The recent large geomagnetic storm characterized by a Kp index higher than 7 is selected for the analysis. It is observed in past studies that the GIVE index for SBAS systems is highly inflated to protect the users against high uncertainty during the storm period.

The analysis method is based on the parameters obtained in the position domain using the gLAB software. For supplementary analysis and interpretation, ESA's SBAS MENTOR tool is used. Information regarding ionospheric events and geomagnetic storms is derived from the public information portal (**Spaceweatherlive, 2023**).

Equations 3-8 are used to compute the protection levels for each data set with a sampling rate of 15 minutes. The protection levels are checked against the ICAO SARPs (**RTCA, 2020**) requirement for various aircraft procedures (RNP 0.1, LPV, LPV-200, APV-I, APV-II, and CAT-I).

As the analysis is done in the position domain, the nearest ionospheric grid points are used to derive the user-specific term $\sigma_{i,UIRE}^{2}$ using the obliquity factor and the GAGAN broadcast GIVE index. This value has spatio-temporal variability and as such both the coverage of system monitoring and the ionospheric activities impact the variance of the given user. During Kp > 7, it is expected that the term is inflated more than in the nominal situation.

For the simulation where the impact of reduced ionospheric activities is assessed, the assumptions of independent, uncorrelated, and zero-mean distribution for individual errors are kept. The errors from the satellite ephemeris and the aircraft local errors are unchanged and only the variance parameter of ionospheric distribution is changed and reflected in the integrity parameter GIVE index. Higher confidence in the ionospheric estimation for IGP surrounding the 85° E 25° N Airspace is simulated. The impact on the protection level and GAGAN availability are discussed in the next chapter.

Results and Interpretation

The vertical protection level (which is the important performance parameter that enables higher precision landing down to auto-landing in GBAS CAT) is not promising to support APV-I

Table 1: The timeframe for the analysis, selected sites and associated satellite and ionospheric events.

Date	Site	Satellite Events	Ionospheric Events	Remark
2022 (01 March - 31 April)	KTM	None	Low Kp < 5	
2022 (01 March)	KTM	None	Low Kp < 5	Low Iono Variance Simulation
2022 (01 March - 07 March)	Delhi	None	Low Kp < 5	
2023 (16 March - 30 March)	Delhi	None	Low Kp > 7	
2022 (01 March)	KZT	Weak confidence	Low Kp < 5	To check MT28 impact

(threshold: 50 m) or APV-II (threshold: 20 m) for Nepalese airspace. From the horizontal and vertical protection level analysis and Stanford analysis (Figure 3 - Figure 6), it is evident that the GAGAN system is currently not suitable to support a precision approach and landing in this region. This is also in line with the recommendation from the Airport Authority of India, that during the nominal ionospheric activities, the GAGAN performances show APV I availability of 99 % of the time over only 76% of the Indian landmass (**AIM, 2023**). The main reasons for the unavailability of APV-I and APV-II are:

a. The higher ionospheric delays and the associated variance for the GAGAN coverage. This has been verified by an experimental test where the satellite broadcast message is modified to have a lower variance for ionospheric grid points (surrounding the 85° E 25° N) in Nepalese airspace. A tool from ESA (SBAS mentor) is used to generate the modified GAGAN messages, and then the horizontal and vertical protection levels are computed. The protection levels are improved with better ionospheric correction confidence. It is an important point to be considered by the aviation authority and related entities that in the next few years the SBAS systems, including GAGAN, will drive towards dual frequency (using L1 and L5) which allows to cancel the ionospheric errors at the user level. Also, the number of monitoring reference stations will increase to have denser coverage (**ICAO, 2022**). Therefore, this simulation to lower the ionospheric errors and variances (close to the situation when there is dual frequency SBAS or better ionospheric coverage and model) gives performance indications mostly triggered by the quality of satellite orbit and clock corrections. Figure 4 (right plot) shows protection levels computed with the simulated data and the improved protection levels are visible mostly around 06:00 to 09:00 UTC (compare against nominal days protection levels in the left plot). The vertical protection levels are reduced below 50 m which supports the APV-I approach.
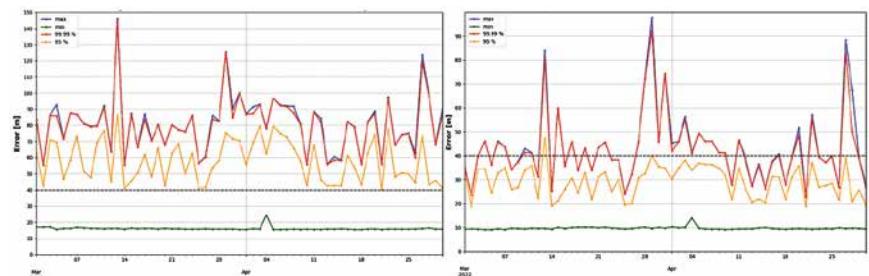
Figure 3: The vertical and horizontal protection levels that can be expected around the Kathmandu airspace.
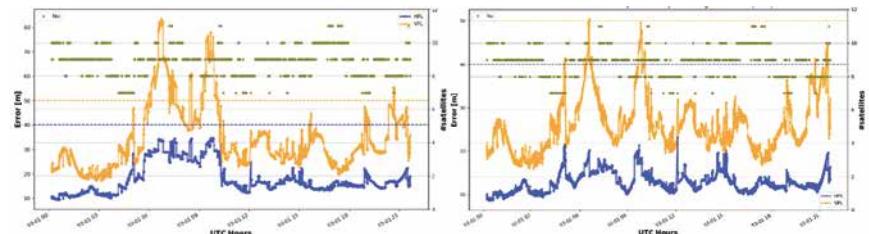
Figure 4: The variability of the protection levels in 24 hours of the day (1st March 2022). The inflated protection levels around 06:00 to 11:00 UTC correlates to the inflated ionospheric variance. Note: the ionospheric content at any location around the globe peaks around 14:00 hour local time. On the right plot, it shows the protection level variability when the confidence in the ionospheric estimation is increased through the GIVE index. It meets the APV–I procedure requirements.
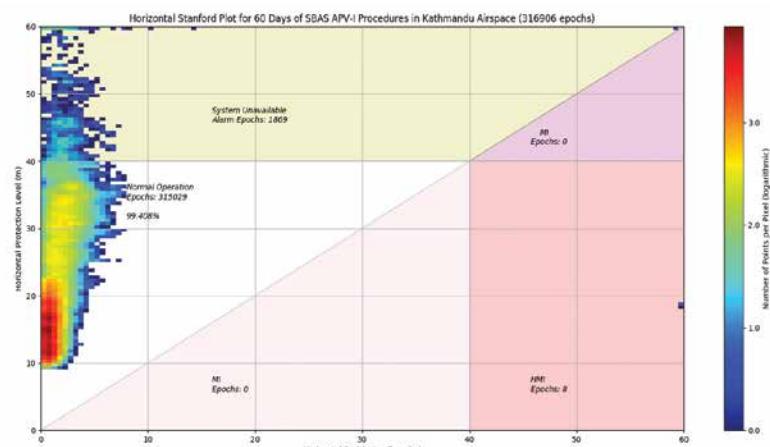
Figure 5: Stanford diagram for HPL for KTM Airport (60 days).
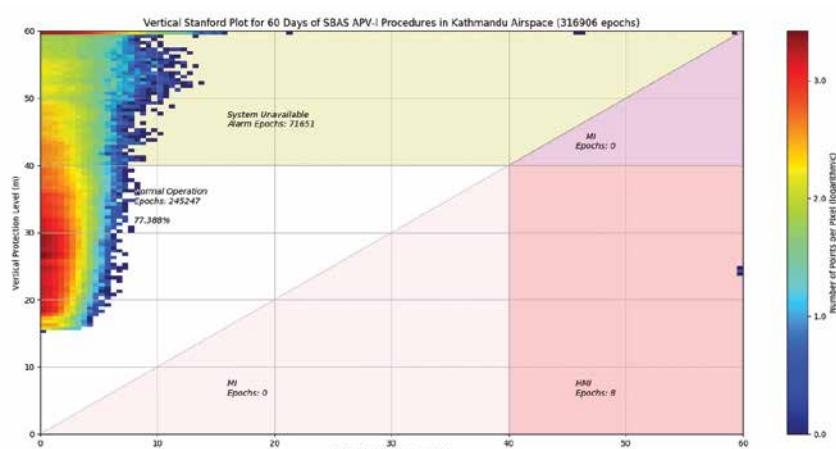
Figure 6: Stanford diagram for VPL for KTM Airport (60 days).

The stanford plots are the established plots to visualize the GNSS system integrity. Figure 5 and Figure 6 show the statistical results for horizontal and vertical navigation using the GAGAN APV-I approach in Nepalese airspace.

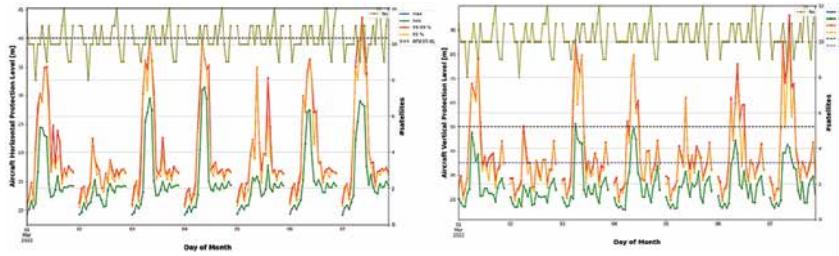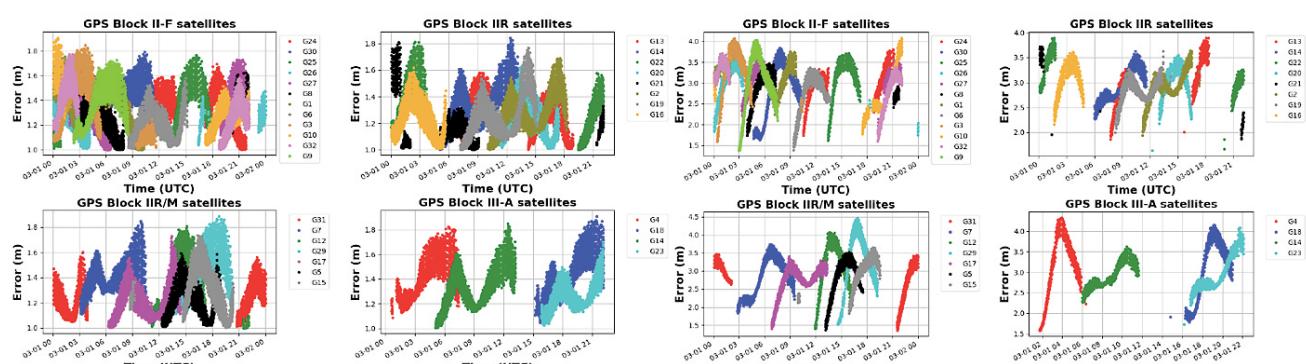As discussed earlier the requirement set by ICAO is not met, mostly due to the degraded performance in vertical domain. The availability of horizontal navigation with 99.4 % shows a great promise for further enhancement of the system. The 8 epochs identified as Hazardously Misleading Information (HMI) are not investigated in detail, as the focus is on the system availability. The vertical availability of 77.3% is a long way off from the required specification. It is well understood that the impact of the ionospheric errors is larger in the vertical position domain. In this regard, the simulation performed earlier (Figure 4) where the ionospheric variance was lowered provided a better vertical protection level. It is also a testament that the GAGAN system holds great potential going forward.

The analysis so far focused on the Nepalese airspace which lies towards the northern edge of the GAGAN coverage. To also analyze the performance which

Figure 7: Performance of protection levels for Delhi Airspace in 2022 (low ionospheric activities Kp index < 4). The horizontal protection level (left plot) meets the APV–I requirement. The vertical protection level (right plot) has a larger variation and does not regularly meet the requirement.
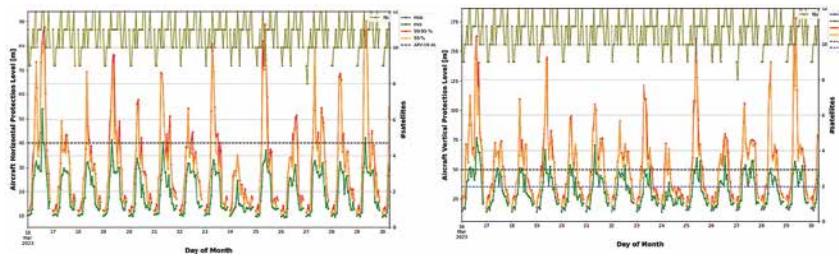
Figure 8: VPL for Delhi Airspace. Performance of protection levels for Delhi Airspace in 2022 and 2023 (high ionospheric activities). The inflation of vertical protection levels during the 2023 Kp index > 7 is visible.
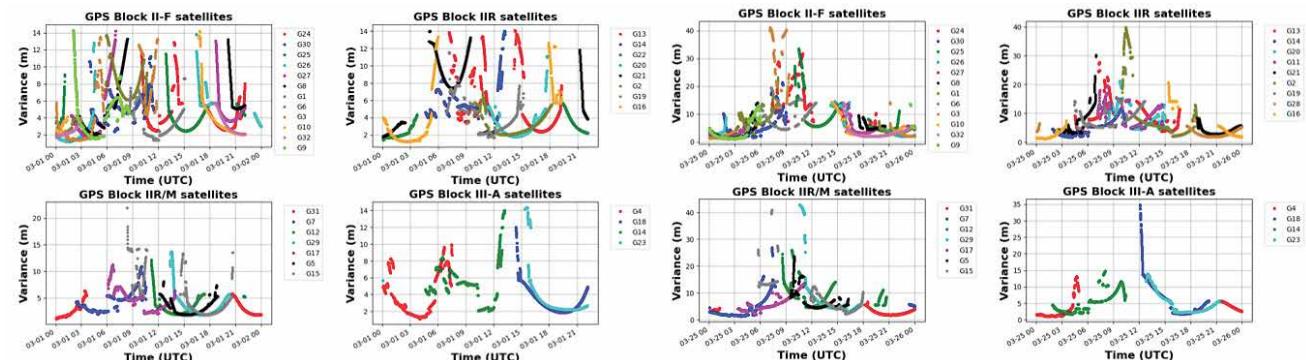
Figure 9: Variability of the ionospheric confidence bound observed by the user in Delhi airspace during nominal ionospheric days and on the Kp index > 7 day. All satellites are impacted by the inflation of ionospheric variance term in the integrity message of the GAGAN.

Figure 10: The satellite observational geometry from the GAGAN network provides better confidence in satellite clock and orbit error corrections for Northern Indian airspace (Left two columns plots). Outside of the coverage, the MT 28 covariance matrix does not improve the confidence but rather degrades it. The right plot (two columns) shows the degraded UDRE observed in Kazakhstan.

is towards the inner coverage, the data from Delhi is analyzed. Both nominal ionospheric days and high ionospheric activity days are used to characterize the performances. Figure 7 and Figure 8 show the variability of horizontal and vertical protection levels. As with the case in Nepalese airspace, the APV-I requirements are not met in nominal days. The performance is degraded to a larger extent during non-nominal ionospheric activities. The overall performance observed in the period used in this study corroborates the public information provided by the Airport Authority of India (**GAGAN, 2023**).

To better understand the large difference in protection level during nominal and non-nominal ionospheric activities, the ionospheric confidence bound is computed for the given location. Figure 9 shows the degraded (two columns plots on the right) user vertical ionospheric error on the high storm day in comparison to the nominal day (two columns plots on the left). All satellites have higher error terms associated to enhanced ionospheric disturbances.

b. The regional network of GAGAN station is not dense as of now (**ICAO, 2022**). There is a plan to increase the network in the surroundings of the Indian subcontinent. This has a direct implication in the performance improvement not only for ionospheric monitoring (better confidence bound in terms of variance) but also well for better confidence bound in terms of satellite orbit and satellite clock error corrections (broadcast through Message Type 28 Covariance Matrix). To experimentally test this, the covariance matrix from MT28 is used to compute the delta User Differential Range Error (UDRE), which is dependent on the location of the airspace from where the aircraft receives the satellite signals. The confidence interval of each satellite orbit and clock error on the line of sight is multiplied with the broadcast UDRE to get the final variance in the protection level calculation (**Walter et. al, 2021**). The better the location of the user w.r.t the observability of GPS satellites monitored by the GAGAN network, the better the

protection level. The UDRE of each satellite from the GAGAN broadcast is the same value for all airspace locations in the GAGAN service volume. However, the delta UDRE is different from one location to the other. Figure 10 shows the delta UDRE for airspace in Kazakhstan and Nepal. The difference is evident, i.e. the observability of satellites from Nepal has more confidence in terms of error as the GAGAN network provides better confidence. Whereas in Kazakhstan, the GAGAN network has lesser observabilities of satellites and hence, weaker confidence.

Comparison with existing systems

As the global SBAS system promotes seamless integration of navigation

procedures from one region to another, it is vindicative to compare the performance of the existing global SBAS system during high solar activities. WAAS and EGNOS are the forerunner providing better services up to CAT-I like approach and landing. Regular performance monitoring and reporting of these systems are publically available. About the MSAS system, the potential has not been fully exploited as it can only support RNP 0.1 procedures. The sparse regional monitoring network and the severe ionospheric conditions are the root causes of it. In this study, the performance of all these SBAS systems experienced service degradation to different levels. EGNOS appears as the quintessential system which has the better availability for both APV-I and AVP-II even during the Kp > 7 events. The slight degradation in the edge of

Table 2: Summary of impacts on the existing SBAS systems.

SBAS System	Kp > 7 Impact	Protection Level Impact	APV I and APV II	Remark
EGNOS – Center	Negligible	Negligible	Available	Robust model with recent software updates
EGNOS – Edge	Minor	Elevated	Available	Poor observation of IPPs
WAAS	Major	Highly elevated	Not available	On the 24th severe impact. WAAS Iono model conservatively inflates the variance
MSAS	Major	Highly elevated	Not available. On nominal days as well, only RNP 0.1 is supported	Large threat space due to sparse RIMS network
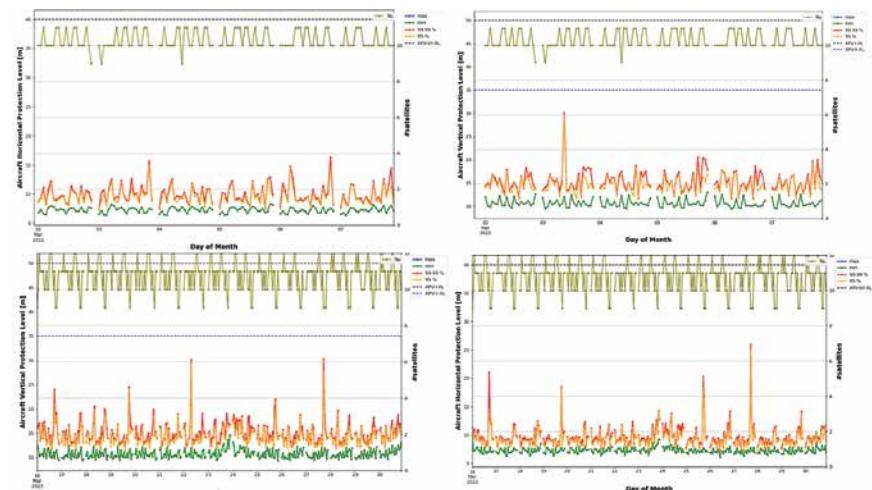
Figure 11: The performance of the EGNOS at the central coverage around Bern, Switzerland. Both horizontal and vertical protection levels for periods in 2022 meet APV-II service requirements. The enhanced ionospheric activities in March 2023 have a minimal impact on the system. APV-II service is met except for the brief period on the 27th of March.

EGNOS coverage, however, is a testament to the necessity of a robust system monitoring that can cover ionospheric irregularities without conservative inflating of the IGPs.

The following plots Figure 11-Figure 15 characterize the performance of protection levels in the position domain computed using the respective SBAS integrity messages for EGNOS, WAAS, and MSAS. The description in each figure caption briefly interprets the results.

## Future evolution and potentials

The safety analysis for SBAS has always encountered the presence of small biases and non-Gaussian behavior observed in data used to validate the system. The analysis performed in this study focused on the integrity equations based on zero-mean Gaussian behavior. And only considered the variance term broadcast from the satellite. Several kinds of literature have corroborated the inclusion of nominal bias terms into the protection level equation to account for non-zero means and non-Gaussian behavior (**Walter et.al, 2009, Walter et.al, 2010, Ober, 2023, Speidel et al, 2013**). A relevant example is the GBAS system which considers the faulted integrity model where bias arising from the ground receivers is also broadcast to the aircraft. As per this literature, the equation 3 formulated earlier in the chapter can be redefined:

$$PL = k_{V/H} \sqrt{\sum_{i=1}^{N} S_i^2 \ \sigma_i^2} + \left| \sum_{i=1}^{N} S_i \ b_i \right| + max \left| S_i \ B_i \right| \quad (9)$$
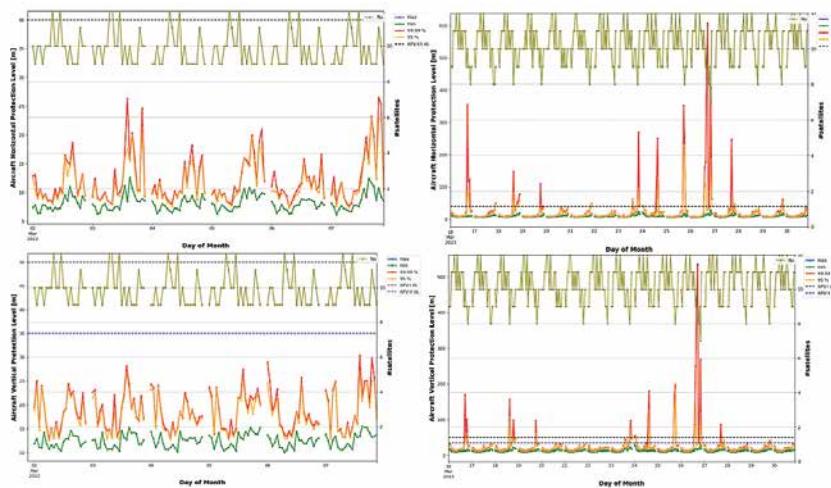
Figure 12: At the edge of EGNOS coverage, in this case, Cadiz in southern Spain, the performance on nominal days is not enough to meet AP–IIV services regularly. The sparse observational geometry in the system requires inflation of ionospheric variance term more often in comparison to the central coverage zone. During high ionospheric activities in March 2023, the inflation is significantly worse than observed in Bern, Switzerland.
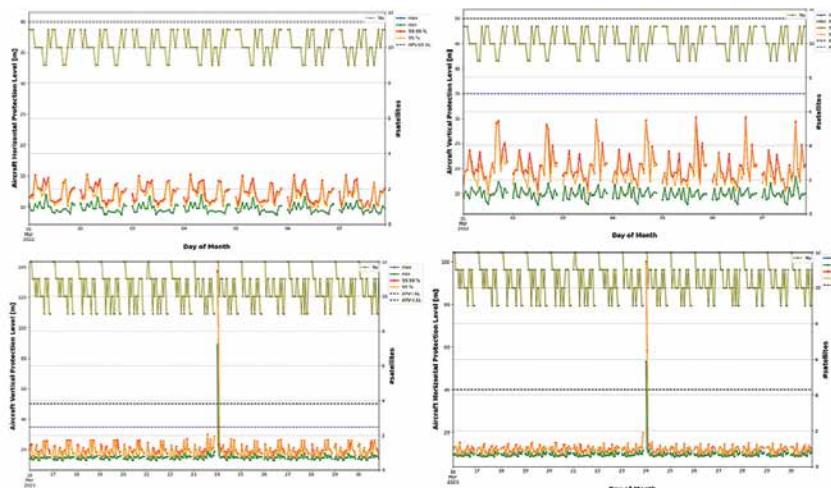
Figure 13: The performance of WAAS observed from New York. In the period analyzed for 2022, APV–II was not met but the LPV and LPV–200 are conveniently met. During the active ionospheric period in March, 2023, the performance looks similar except for the beginning of 24th March where the inflation of variance was quite high that render the service degradation.

here the element of S is taken from the projection matrix, is the nominal variance, and is the nominal bias term. The last term takes the largest bias during the fault event. In the case of the fault-free scenario, this term vanishes. The scalar factor represented can be optimized to get it well below 5.33 and consequently minimize the protection level values (**Walter et. al, 2010**). The bias term can also be isolated per differentiated parameters such as the ground receivers' errors and satellite errors. And the maximum value of the protection level from the possible scenarios is used to protect the user aircraft.

When the DF system is considered, the ionospheric variance term, except for the higher-order ionospheric terms, is eliminated in equation 4 (**Ober, et. Al, 2023**). It has to be noted that the uncertainty in the ionospheric computation is the major source of the degradation of the GAGAN availability for APV-I and APV-II. The opportunity of the DF system (**ICAO, 2023**) will certainly provide better performances. Add to it the robust approach to consider the individual bias term rather than the conservation inflation of the variance as shown in equation 9, and the prospect of GAGAN-based aircraft approach procedures is very promising.

The ICAO has recently adopted the Galileo constellation for the provision of GNSS-based air navigation services (**EUSPA, 2023**). This allows to use of dual constellation in the augmentation system such as SBAS. The implication in the protection level is that more satellites and
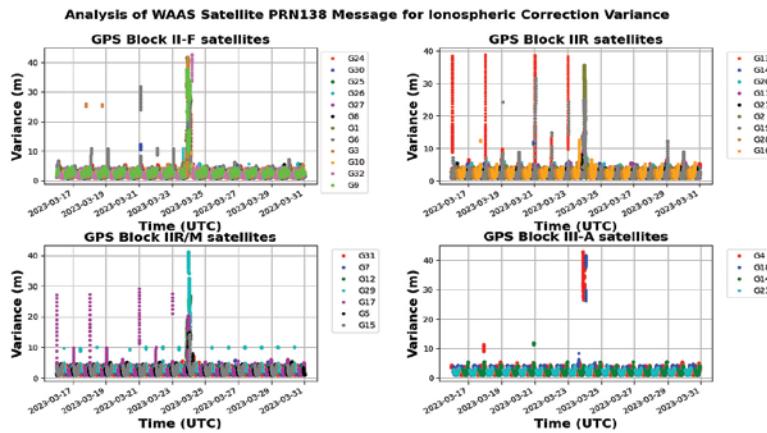
Figure 14: The ionospheric variance term per satellite observed from New York for WAAS from 17th to 31st March 2023. On the beginning of the 24th March, a strong Kp index= 7.4 was reported and it had an impact on the confidence bound of the ionospheric corrections. It was significantly inflated for all satellites. The service degradation for this period is well documented in the FAA WAAS performance analysis report (FAA, 2023).
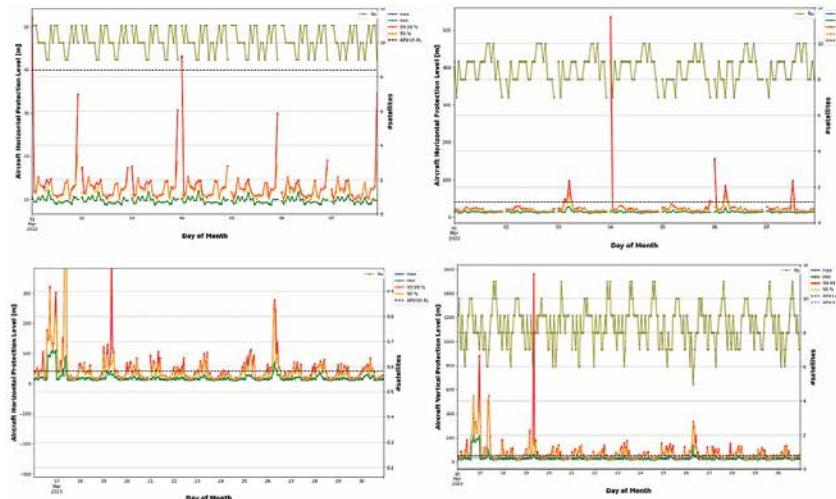

Figure 15: The performance of the MSAS system as observed from Japan shows a severe limitation to support APV–I and APV–II services. On nominal days in 2022, the system was able to support RNP 0.1 procedures with one exception on the 4th of March. During strong ionospheric activities in March 2023, the system was significantly degraded with several days unable to support RNP 0.1 procedures as well.

signals are available which improves the satellite user geometry and as per equation (3-8) the protection level values are lowered rendering better availability of APV-I and APV-II.

The potential of more precise carrier-phase signals has been studied in the past and could be the subject of investigation in the coming years as well. The inherent challenges of the carrier phase, such that cycle slips and phase ambiguities, however, hinder the implementation in safety-critical systems

with high requirements of integrity (**Du, 2021**). A-RAIM with DFMC is also a promising approach and its success could also benefit the evolution of the SBAS algorithm. The A-RAIM concept is based on the local integrity computation where the pseudo-range from all satellites is statistically checked to detect and isolate the faulty satellite. It has also been demonstrated in literature the possibility of using a particle filter that can provide better results for the non-zero-mean non-Guassian error model.

Conclusion

The study provided an assessment of GAGAN services for APV-I and APV-II over the Indian territory. Satellite error bounds and ionospheric error bounds are analyzed as the main contributing integrity parameters. It is observed that during nominal periods the protection level performance requirements of APV-I are mostly met but still not enough to meet the 99.99% availability requirement. It is still a far-fetched goal to meet the APV-II requirement. During the enhanced ionospheric activities triggered by geomagnetic storms with a Kp index > 7, the protection levels are highly inflated to protect the users at the expense of service availability. With simulated data, it is verified that lowered ionospheric variance improves the performance and regularly meets the APV-I requirement. The well-established EGNOS and WAAS provide better services including LPV, LPV-200, APV-I, and APV-II. At the edge of EGNOS coverage, the performance is not as robust, and inflation of ionospheric variance is frequently triggered. The WAAS system also experienced a short interruption in service availability on the 24th of March, 2023 during the high Kp index period. MSAS is currently only serving RNP 0.1 approach and hence, it is expected to have very large protection levels during the ionospheric events. Some insights were provided into the potential development of DFMC and a less conservative integrity approach that includes an individual bias term.

Acknowledgment

Disclaimer

The work done in this study has no commercial interest. It is the author's

voluntary support to facilitate the GNSS capacity-building activities in the framework of ICG, UNOOSA agenda. There was no funding received and no support was used from any organizations. The analysis, interpretation, and discussion are solely based on the author's expertise in GNSS and air navigation.

It is observed that during nominal periods the protection level performance requirements of APV-I are mostly met but still not enough to meet the 99.99% availability requirement. It is still a far-fetched goal to meet the APV-II requirement. During the enhanced ionospheric activities triggered by geomagnetic storms with a Kp index > 7, the protection levels are highly inflated to protect the users at the expense of service availability

References

AAI (2023), https://gagan.aai.aero/gagan/

GAGAN (2023), https://gagan.aai.aero/gagan/content/apv-1-rnp-01-services

AIM (2023), https://aim-india.aai.aero/eAIP_Archive/18-05-2023/eAIP/IN-ENR%204.3-en-GB.html

Du Y, Wang J, Rizos C, Mowafy AE (2021),Vulnerabilities and integrity of precise point positioning for intelligent transport systems: overview and analysis

EUSPA (2023), New Achievement for Galileo and Civil Aviation, https://www.euspa.europa.eu/newsroom/news/new-achievement-galileo-and-civil-aviation

FAA (2023), Wide Area Augmentation System Performance Analysis Report April 2023, Report #84, https://www.nstb.tc.faa.gov/reports/FAA_WAAS_PAN_Report_84_v1.0.pdf

Gupta S, Gao G, (2021), Reliable GNSS Localization Against Multiple Faults Using a Particle Filter Framework

ICAO (2023), GNSS milestone achieved as ICAO Council adopts new dual-frequency multi-constellation standards, https://www.icao.int/Newsroom/Pages/GNSS-milestone-achieved-as-ICAO-Council-adopts-new-dualfrequency-multiconstellation-standards.aspx

ICAO (2022), GAGAN Regional Service Availability, https://www.icao.int/APAC/APACRSO/GBASSBAS%20Implementation%20Workshop/3-7_GAGAN_Regional_Service_Availability%20(T%20Schemmp).pdf

ICAO (2016), Asia Pacific Office, SBAS safety assessment guidance related to anomalous ionospheric conditions

Indiatimes, https://economictimes.indiatimes.com/industry/transportation/airlines-/-aviation/indian-aviation-market-has-huge-potential-waiting-to-be-tapped-top-industry-experts/articleshow/101857232.cms

Insidegnss (2016), https://www.insidegnss.com/auto/janfeb16-GAGAN.pdf

Insidegnss, (2020), Why is bounding GNSS errors under rare or anomalous conditions important, and what makes it difficult?

Navipedia (2006), The SBAS Integrity Concept Standardised by ICAO: Application to EGNOS

Ober PB, Farnworth R, Breeuwer E, Willigen D (Accessed: 2023), Overbounding the SBAS Integrity Equation

PIB (2015), https://pib.gov.in/newsite/PrintRelease.aspx?relid=123209

PIB (2022), https://pib.gov.in/PressReleasePage.aspx?PRID=1820947

Sophan S, Myint L, Saito S, Supnithi P (2020), Performance improvement of the GAGAN satellite-based augmentation system based on local ionospheric delay estimation in Thailand

Spaceweather (2023), https://www.spaceweatherlive.com/en/archive.html

Sparks L, Altschuler E, Panday N, Blanch J, Walter T (2021), WAAS and the Ionosphere-A Historical Perspective: Monitoring Storms

Speidel J, Tossaint M, Wallner S, Rodriguez JA (2013), Integrity for Aviation: Comparing Future Concepts

RTCA (2020), RTCA DO-229 Minimum Operational Performance Standards (MOPS) for Global Positioning System / Satellite-Based Augmentation System Airborne Equipment

Walter T, Hansen A, Enge P (1999)Validation of the WAAS MOPS Integrity Equation

Walter T, Hansen A, and Enge P (2001), Message Type 28

Walter T, Blanch J, Enge P (2010), Vertical Protection Level Equations for Dual Frequency SBAS

Walter T, Blanch J, Rife J (2004), Treatment of Biased Error Distributions in SBAS

Walter T, Blanch J, Enge P (2009), Evaluation of Signal in Space Error Bounds to Support Avaition Integrity

Yun Y, Kim D, Kee C, (2006), A Particle Filter Approach to DGNSS Integrity Monitoring- Consideration of Non-Gaussian Error Distribution

Zu N, Marais J, Betaille D, Berbineau M, (2018), GNSS Position Integrity in Urban Environments: A Review of Literature

An architecture for a visual-based PNT alternative

This work illustrates implementation using the simple architecture of a star tracker camera. Known as CROSS, the technology is a new navigation tool in development by the University of Sydney

Joshua J.R. Critchley–Marrows
The University of Sydney, Sydney NSW 2006, Australia

Xiaofeng Wu
The University of Sydney, Sydney NSW 2006, Australia

Iver H. Cairns
The University of Sydney, Sydney NSW 2006, Australia

Abstract

This paper treats the problem of positioning and navigation in the absence of GNSS. Given recently raised vulnerabilities for GNSS both on Earth and in space, the work revisits the old problem of the sextant in new light. The combination of stars and planetary horizons was the popular tool for autonomous navigation on-board spacecraft, but given the rise of GNSS receivers, this solution has been largely disregarded. New spacecraft missions beyond Earth have made new progress in visual-based navigation. The work utilises these new methodologies in the scenario that RF-derived positioning is unavailable, achieving a performance below 100 m.

An additional important consideration is the development of new navigation infrastructure in LEO and the Moon. Current methods seek to use GNSS and RF-derived sources for orbit determination, however, to be seen as 'redundancy infrastructure' for critical Earth and beyond applications, these signals cannot be the primary and only source of navigation reference. This paper utilises derived performances for visual-based methods and applies them to the ranging service problem. Most user scenarios in maritime, aviation and lunar domains are satisfied.

This work illustrates implementation using the simple architecture of a star tracker camera. Known as CROSS, the technology is a new navigation tool in development by the University of Sydney. As a star tracker is common device to many spacecraft platform, it simplifies implementation, given that redundant systems are always not a priority to the manufacturer.

1. Introduction

The security and authenticity of Position, Navigation and Timing (PNT) for management of Low Earth Orbit (LEO) satellites has never been more crucial. With the growth of enormous mega constellations, and the increased activity of malicious actors in the space arena, PNT systems need to be strengthened.

Radio Frequency (RF)-derived is the dominant PNT source being used in space today, leveraging off Global Navigation Satellite Systems (GNSS) and ground tracking infrastructure. Even though these mechanisms are highly accurate, they are also easily jammed and spoofed from malicious sources, as well as being limited in coverage and availability. Utilising visual-based methods can be more reliable and not as restrictive.

Stars and celestial bodies have long been considered separately in attitude determination applications [1–6]. However, a combination of these sources are now being considered for positioning, where operating in tandem provides an ability for relative positioning to the celestial body centre [7–13].

Recent missions have successfully used celestial navigation for the purposes of orbit determination, target tracking and rendezvous. Such missions include Hayabusa 2, which employed single target tracking at long distances and artificial landmark navigation on approach [14]. Similar approaches have been developed and successfully operated on DART [15] and OSIRIS REX [16] missions.
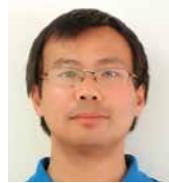
Even though missions have been successful in the use of visual-based navigation for relative positioning to small celestial objects such as asteroids, delivering an visual-based navigation system for absolute positioning is not as well developed. However, as mentioned, the need for alternatives to RF-derived positioning is necessary.

Some recent early stage studies have evaluated the use of the plan- etary body limb for the Earth orbit determination problem [10,17]. However, more successful results have been achieved for the case of the Moon [12,18,19]. The approaches developed for the Lunar scenario are treated for the Earth, as was initially adopted in Ref. [20].

This issue is especially challenging for the case of Earth due to the atmosphere, which develops a non-constant offset to the measured ho-rizon. This issue is not developed in the literature, as noted in Ref. [21]. It is also present in other planetary systems of interest for exploration, such as Mars. This paper presents a potential to this problem.

An additional challenge presented to the navigator is miscalibration in the optical lens system. Star trackers are often employed to solve this problem [22]. The paper proposes solutions to this issue also modelling the effect of the Earth albedo effect.

Table 1: Domain performance expectations for navigation.

User	Domain	Accuracy	Time-to-alert	Comments	References
Aviation	Oceanic	7.4 km	5 min	Abstracted from alert limits.	[33]
	Continental	3.7 km	5 min		
	Terminal	1.85 km	15 s		
	Approach	556 m	10 s		
Maritime	Oceanic	1 km	1 min		[34]
	Coastal	100 m	30 s		
	Port Approach	10 m	10 s		
	Port	1 m	10 s		
	Inland Waterways	10 m	10 s		
Terrestrial Space	SAR	635 m	–	Derived from a 7400 km operating altitude	[35]
	LEO Broadband	100 m	–	More based on	[36]
	Geostationary	1 km	–	technology limitations rather than system performance delivery.	
	Space Traffic	500 m	–		[37]
Lunar Space	Lunar Transfer	13 km	–		[38]
	Orbit	1 km	–		
	Initial Descent	300 m	–		
	Final Descent	100 m	–		
	Surface Position	10 m	–		
	Lunar Gateway Rendezvous	500 m	–		

The paper presents the potential performance of a visual-based PNT infrastructure for mega-constellations. Not only may this provide an alternative source of orbit determination reference for the spacecraft in orbit, but it might be also leveraged by future navigation constellations to support ranging services for terrestrial and lunar users. This future infrastructure is commonly coined LEO GNSS [23,24] and Lunar Communication and Navigation Satellites (LCNS) [25–27]. It is a requirement in various industries that any alternative service cannot rely on GNSS, and so it is a requirement that an orbit determination capability must be independent [28,29].

The novel nature of the work is presented by the following points:
- A complete and practical assessment to the use of visual-based navigation to support future ranging navigation infrastructure.
- A review of PNT requirements from terrestrial critical transport users and operators, as well as Earth-orbiting satellites and lunar spacecraft.
- A solution to the atmospheric offset problem for visual-based navi-gation in LEO. This may also be applied to other planetary bodies that may contain an atmosphere.
- An approach to multiple attitude and navigation camera systems, as well as an assessment to the effect of Earth albedo on star detection and misalignment correction.
- A performance evaluation for the introduction to LEO ranging infrastructure around the Earth, including a novel approach to its predicted performance.

The paper starts by introducing the PNT landscape, illustrating the various required performances for both in-orbit satellites and terrestrial users of a space-based ranging service. An architecture is then introduced for position determination utilising visual-based references. After presenting and discussing the potential performance, this method for orbit determination is considered as part of a new type of GNSS-like ranging service.

2. The PNT landscape

PNT information is essential for most modern technology, from navigating ships and aircraft to providing time of transaction recordings for the financial market. The adoption of PNT across market sectors has been well considered within the literature [30–32]. Many articles especially emphasise the need for robust PNT across each domain, assuring its availability and integrity.

Given the importance of this information for system integrity, separate industrial bodies and organisations have captured minimum performance requirements for their respective technologies. Four different domains are reviewed in this paper, across aviation, maritime, terrestrial and lunar space, to understand target performance requirements that are required by a visual-based navigation alternative.

These requirements are driven with respect to both primary and back-up related PNT infrastructure, that

should be assured for the sys-tem to act responsibly. The performance requirements are captured in Table 1.

2.1. Aviation

The aviation industry is very strict when considering the user segment, given the safety-of-life criticality of their application. Because of the raised vulnerabilities of GNSS, pilots are instructed that such instruments should not be used as their primary source of position information. Instead, radar, ground tracking, and even human-derived visual feature recognition should be employed by the pilot.

The user requirements for navigation may be derived by the integrity alert limits by airspace, these being the limit to navigation accuracy uncertainty before an alert is issued. The integrity alert limits for GNSS, derived from the GNSS Manual [33] issued by the International Civil Aviation Organisation, are used in Table 1 as the absolute minimum expected performance for an aviation navigation unit. For most segments of the aeroplane voyage, excluding those of final approach, the user should hold a 500 m confidence in their position.

2.2. Maritime

The maritime industry maintains less strict requirements for navigation than aviation. However, the maritime sector has been subject to some of the most extreme jamming and spoofing attacks of recent years. One such series of event was exposed in a study by the Centre for Advanced Defence Studies [39]. Focusing on GPS spoofing attacks in Russia and Syria, cases were reported in the Black Sea and Syria where cargo ships reported their position several miles outside of Moscow. Similar events have also been reported in the Port of Shanghai, China [40], as well as around the Red Sea [41].

In response to these malicious attacks, as well as other sources of disruption to GNSS, the International Authority of Lighthouse Authorities derived a suggested list of minimum maritime user requirements for each phase of a voyage [34]. The measures also include system integrity requirements, which were discussed in Section 2.1 on aviation. The suggested performances are summarised in Table 1. It should be noted that the cruder performances are permitted during the ocean and coastal phases of a voyage, where accuracies of less than 100 m are required. This is within an absolute frame, and so dead reckoning based systems would not be feasible.

The definition of a back-up system is a key output of [30] a system that 'ensures continuation of the navigation application, but not necessarily with the full functionality of the primary system and may necessitate some change in procedures by the user.' By this definition, if GNSS become inoperable, such a backup system must be available to fulfil this need. The back-up system would require 99% availability [34], so terrestrial infrastructure providing a ranging signal would not be suitable.

2.3. Terrestrial space

Most requirements for Earth-orbiting satellites are driven by the technology capability rather than the needs of the application [36]. Performances given in Table 1 consider applications of Synthetic Aperture Radar (SAR), LEO broadband constellations and geostationary communication satellites.

Even if their performances might not be met for the primary mission, back-up or redundant systems are helpful to ensure system reliability. For tracking and monitoring of space traffic, as well as space situational awareness applications, accuracies are typically at the 0.5 km mark [37], achieved through basic ground-based tracking techniques. Supplementing this with an autonomous on-board system would be beneficial to reduce dependency on expensive radar infrastructure, as well as ensuring the system is self-reliant.

An important topic of this paper is the application of visual-based PNT to the delivery of LEO PNT services. This is considered a different category of requirement to those discussed in this section, and so is treated as part of the system analysis in Section 4.

2.4. Lunar space

Lunar navigation requirements have been summarised in recent in-ternational space agency documentation. It is seen that navigation infrastructure is required to support future missions to the Moon, as an increasing number of private organisations seek travel. Needs are captured in initiatives such as Moonlight by the European Space Agency (ESA) [42], and LunaNet by NASA [38]. These efforts have captured requirements for different mission phases, driven by a motivation that current systems are insufficient.
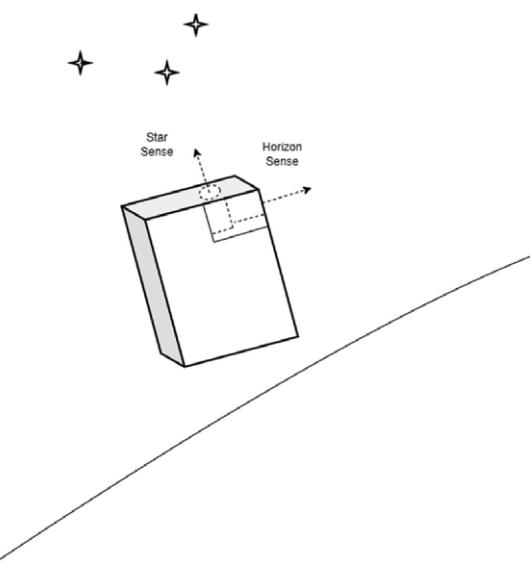

Fig. 1. Illustration of the visual–based navigation concept for a spacecraft in orbit.

The requirements treated by NASA's LunaNet and associated infrastructure for each mission phase are summarised in Table 1 [38]. Most phases require performances up to 100 m, which might be met by the visual-based PNT architecture outlined in Section 3.

The delivery of navigation services from lunar orbit may also utilise visual-based PNT for orbit Determination. Section 4 concentrates on the delivery of terrestrial PNT services, but this might be extrapolated for lunar environments.

Table 2: Parameters of the CROSS star tracker.

Parameter	Value
Cross-Axis Accuracy	24″
Boresight Accuracy	18″
Angular Rate Accuracy	4.40″/s
Star Catalogue Size	2.8 GB
Star Brightness Cut-off	5.0
Sky Availability	99%
Sun Exclusion Angle (SEA)	50°
Field of View (FOV)	20°
Image Dimensions	2448 × 2048 px
Size (Camera Assembly)	60 × 54 × 50 mm
Size (CPU and PCB)	98 × 67 × 14 mm
Mass	235 g
Voltage	5V
Power (Nominal)	2.5W
Power (Peak)	4.5W
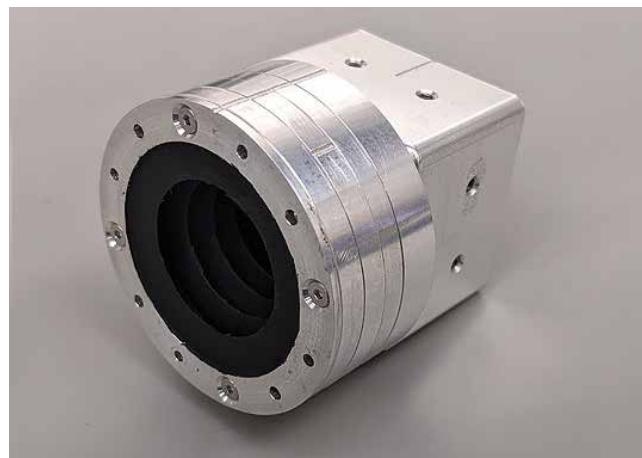
Fig. 2. CROSS Star Tracker in the laboratory.
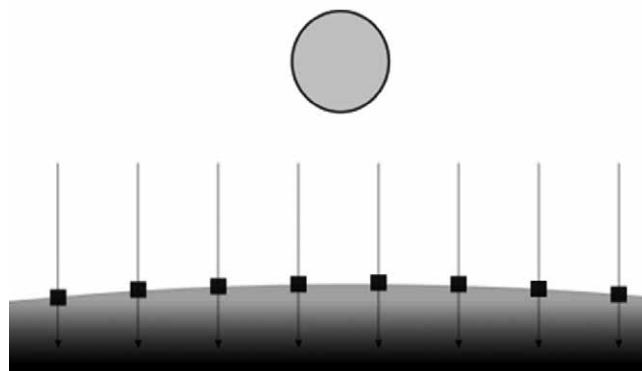
Fig. 3. Horizon edge identification by strip search.

3. A proposed alternative

This section evaluates the expected performance and challenges of a visual-based PNT alternative. The proposed technology is considered in context of operational environments discussed in Section 2.

Visual-based refers explicitly to the visual band of the electromagnetic spectrum. Measurements of this kind are typically observed by a camera. Given the nature of visible sunlight, stars and their visible band emissions (450–800 nm), both direct and indirect observations, such as through reflection, can be used as a permanent natural form of navigation reference. These statements should be obvious for the reader, and clearly humans constantly use this type of medium for navigating our own environment. The important point is that this is an alternative to GNSS/RF-based positioning sources, which rely on man-made infrastructure and are more simple to manipulate and deceive [35].

For a spacecraft or ship, disrupting a camera would require a very close or extremely powerful light emitting device to interfere with the observation, and so these navigation references are a powerful alternative. This is not to say they are a replacement. As discussed in Section 2, the focus is to have a resilient back-up to RF-based navigation. It should be note that the current state-of-art visual navigation systems are two orders of magnitude worse than their RF-based equivalents.

Introduced is a proposed architecture for a visual-based navigation alternative. The concept is not novel. As discussed, for the last 60 years, many engineers and scientists have proposed, developed and successfully demonstrated sextants, star and horizon trackers, deep space optical navigation sensors and visual-light ranging devices. However, the adoption of these technologies as an alternative or back-up system for RF-defined environments has not been treated.

Aspects of the approach are assessed by using real space captured image sets, simulated Earth and star lighting environments, and modelling of the orbit trajectory, introducing realistic error parameters. Each analysis independently describes the data used to calculate and present performance of the proposed methodology.

3.1. Concept of operations

The vision-based concept consist of an optical assembly of at least two sensors. Each sensor will point orthogonally, either directed at the celestial body horizon or a star field. The purpose is to capture measurements from each observed object to derive a position reference.

An illustration of the concept is presented in Fig. 1, treating a spacecraft in orbit. 'Star sense' operates as an attitude sensor, providing an orientation between the inertial, celestial

frame of the stars and the sensor body, and 'horizon sense' provides information on the desired body origin reference.

Different terminology is adopted to not confuse the reader with the traditional, separate attitude sensors. This is especially the case for horizon sense, which usually acts as an attitude determination instrument. However, to derive inertial reference frame information, a position in space is also required. The methodology proposed here operates in reverse.

The optical navigation sensor architecture is developed using an initially purposed star tracker made by the University of Sydney. Known as CROSS, a wide field of view optical assembly and baffle supports a high performing attitude determination reference for a CubeSat architecture [43,44]. This same architecture is treated here for the combined star and horizon sening architecture.

The properties of the CROSS star tracker are summarised in Table 2. The same sensor assembly will also be utilised for 'star sense'. For 'horizon sense', a slight increase in FOV is used, from 20∘ to 40∘. A baffle is not necessary for 'horizon sense' as observations of the Moon and Earth are desired, and are not treated as stray light sources to observing stars. A picture of CROSS is shown in Fig. 2.

It should be noted that an infrared-band sensor might also be considered, permitting much more sustainable operations in eclipse. It has also been discussed in previous work that the atmosphere is at a near constant height elevation in this band [21]. However, this work is limited to considering the visible light bands utilising the architecture of a star tracker. An infrared sensor is a topic of further work.

3.2. Implementation methodology

The operation algorithms include star tracking alongside attitude determination, horizon identification and position localisation. Measurement are combined within a Kalman filter to improve performance, which is quite substantial. These steps are not presented in detail, but the main ideas and results are outlined. The reader is referred to recent work in the literature with the introduction of each topic.

3.2.1. Attitude determination

The operation of the star tracker within the scope of optical navigation is not discussed in this paper, as the topic is very mature. The reader is referred to state-of-the-art publications on the topic of star trackers [4,5,44,45].

To summarise the core algorithms implemented, the methodology is as follows:
1. Image is captured by star sense.
2. Filter image using a Gaussian/blur kernel.
3. Establish bright pixel/star threshold and search image for stars.
4. Generate regions of interest around each pixel.
5. Calculate star centre by moment method centroid.
6. Identify stars by use of TETRA algorithm [46].
7. Calculate attitude by identified stars celestial frame vectors and measured body vectors by Davenport q-method [47].

The attitude is then combined with the measured horizon edge localisation to produce a position estimate.

It might be considered helpful to include the star centroid estimates directly into the position localisation algorithm, where an output would include both attitude and position information. However, the horizon model also includes orientation information. Even if the horizon identified points are weighted relative to the stars, as the horizon is much less accurate than the star measurements, studies by the authors that the loss in accuracy is significant. So, the process of attitude and position determination is decoupled.

3.2.2. Horizon edge identification

As with star tracking, the topic of horizon sensing for attitude determination is a mature topic. Early horizon sensors approximated the horizon to a flat line, given the planetary geometry measured close to the Earth surface. With leapfrog advances in camera technology and processing, horizon identification and approximation has treated with ever greater detail the observed conic geometry.

Identification and sub-pixel localisation of the point series treated in this work considers the well-developed approach of [18]. This approach is summarised in a series of steps:
1. Identify the direction of sunlight to the planetary body.
2. From the image corners, draw a series of lines running along the direction of illumination. This step is illustrated in Fig. 3.
3. When the line encounters a bright pixel greater than a certain threshold, commence counting to the number of subsequent pixels that also exceed
4. This threshold.
5. If the number of bright pixels exceed a minimum count, then create a region of interest around the pixels.
6. By use of a Sobel-based gradient kernel, identify the pixel in the region where the increase in intensity across pixels is greatest.
7. Create a new region around the desired pixel, and apply a Zernike moment on the region to identify the sub-pixel where intensity change reaches its peak.

To demonstrate the expected performance, an additional step is introduced. A hyperbola is fitted to the located pixel points. The Fitzgibbon conic section fitting technique is used for this [48]. This is combined with a RANSAC outlier rejection methodology [49].

The performance of the horizon edge localisation is assessed using an image sourced from NASA from the orbit of the

International Space Station [50]. The image contains the same pixel resolution as the CROSS camera sensor specified in Table 2. Even though the optic assembly is different, the precision demonstrated is assumed comparable.

The results are presented in Fig. 4. The precision of the fit is esti-mated to be approximately 2 px when calculating the root-mean-square error. This error is caused primarily by camera-related noise. This pre-cision will be utilised in the subsequent analysis of Section 3.4.

An important consideration is the atmospheric offset, which might be abstracted from Fig. 4 given the uncertainty in discerning what might be clouds or atmospheric illumination, and what is the horizon body. This is a topic of discussion in Section 3.3.2.

3.2.3. Position localisation

Position estimation using the measured planetary horizon is an often revisited topic. The topic has re-emerged recently as part of recent efforts led by NASA to revisit the Moon. NASA set a requirement for their Orion crewed module that it must operate autonomously in *cis*-Lunar space. Recent developments and approaches include [9,19].

The measured horizon, as introduced in Section 3.2.2, is either measured as an ellipse, circle, parabola or hyperbola, depending on the orientation of the camera. All are conic sections, and so may be treated by the general form,

$$Ax^2 + Bxy + Dy^2 + Ex + Fy + G = 0, \qquad (1)$$

where $\{A, B, D, E, F, G\}$ describe the shape of the conic section and (x, y) are coordinates in the two-dimensional image plane.

This expression might also be described in matrix form,

$$s^T C s = s^T \begin{bmatrix} A & B & E \\ B & D & F \\ E & F & G \end{bmatrix} s = 0, \qquad (2)$$

Fig. 4. Horizon edge localisation for an Earth horizon image, with the fitted line shown in red. The precision is estimated to be 2 px. (For interpretation of the references to colour in this figure legend, the reader is referred to the Web version of this article.)

where the conic sections parameters have been arranged within a matrix, C, and the image pointing vector is described by $s = \{x, y, 1\}^T$.

The general shape of an ellipsoid can be described by a surface pointing vector p and a shape matrix $A = \text{diag}\left\{\frac{1}{a^2}, \frac{1}{b^2}, \frac{1}{c^2}\right\}$. In a reference frame aligned to the planetary object, this relationship is given by,

$$p_P^T A_P p_{p=P} = 1, \qquad (3)$$

where subscript P indicates the planetary frame. Relationship between the surface pointing vector p and observed horizon point vector s is given by the sensor position, r, as,

$$p_P = r_P + ts_P, \qquad (4)$$

where t is a scaling parameter. Combining Eqns. (3) and (4) then produces an expression for the horizon measurement vectors s and a new matrix, M,

$$s_P^T M s_P = 0, \qquad (5)$$

where $M = Ar_P r_P^T A - (r_P^T A r_P - 1)A$. Consider the fact that the horizon points are given in the planetary frame, so these can be transformed by an attitude matrix from the body B as,

$$s_P = T_{PB} s_B, \qquad (6)$$

where the attitude T_{PB} is known from the 'star sense' determined attitude alongside a combination with planetary orientation parameters. Planetary orientation parameters provide attitude information between inertial I and P frames, T_{PI}, and the star derived attitude provide orientation between B and I, T_{IB} so the complete relationship is,

$$T_{PB} = T_{PI} T_{IB}. \qquad (7)$$

There are many static, least square solutions to (5) problem [19,51], but the most successful is the Christian-Robinson method [11] which applies a Cholesky parameterisation to the expression in Eq. (5), simplifying the form to a linear least square problem.

3.2.4. Kalman filter

The problem produced in Section 3.1.3 can be solved in a Kalman filter. The implementation is outlined here and will be detailed else-where [20]. Given the non-linear nature of Eq. (5), the Extended Kalman Filter (EKF) is used.

As mentioned in Section 3.1.1, the star tracker attitude determination problem is solved separately. The state and measurement vectors are then given by,

$$x = \left\{r^T \ v^T\right\}^T, y = \left\{s_1^T \dots s_m^T\right\}^T, \qquad (8)$$

with vector y containing the m measured horizon points.

The typical implicit EKF procedure is then implemented, following sequence of operations,

$$x_k^- = f(x_{k-1}^+), P_k^- = F_k P_{k-1}^+ F_k^T + Q_k, K_k = P_k^- H_k^T (H_k P_k^- H_k + R_k)^{-1}, x_k^+ = x_k^- \quad (9)$$
$$+ K_k h(x_k, s_k), P_k^+ = (I_6 - K_k H_k) P_k^-,$$

where k and $k\text{-}1$ are the current and previous state, P is the state covariance matrix, Q is the propagation noise matrix, R is the measurement noise matrix, K is the Kalman gain and I_6 is the 6×6 identity matrix. Functions $f(x)$ and $h(x, s)$ are the modelled relations for propa-gation and measurements respectively. The observation function for the horizon is simply given in Eq. (5), so for the i th horizon point,

$$h(x, s_i) = s_i^T M(r) s_i = 0. \quad (9a)$$

The h vector is constructed using the set of m points. The equivalent Jacobians for the two functions $f(x)$ and $h(x, s)$ are,

$$F_k = \left[\frac{\partial f}{\partial x}\right]_{x=x_k}, H_k = \left[\frac{\partial h(x, s)}{\partial x}\right]_{x=x_k}, \quad (10)$$

that produce the state transition and observation matrices, respectively.

The propagation step would consider a simple orbit propagation model. Given the expected performance is on the order of hectometres, the modelling is limited to considering the gravitation force vector only. Other force elements are assumed negligible at this order of accuracy. The spacecraft acceleration $\ddot{r}$ is calculated as,

$$\ddot{r} = -\frac{\mu}{r^3} r, \quad (11)$$

where μ is the gravitation constant proportioned to the planets mass. The state transition matrix F may then be simply estimated by taking the derivative, and the propagation $f(x)$ is implemented through Runge- Kutta integration of the gravitation acceleration differential equation.

3.3. Challenges

This section briefly discusses two major challenges for the proposed system. The first is the calibration of misalignment between the two sensors, and the effect stray light might have. The second is the bias in the observed horizon compared to the planetary ellipsoid, caused by the atmosphere. Both these issues have been ever present in vision-based position determination [9]. Presented are methodologies that hold po-tential to overcome these challenges.

3.3.1. Misalignment calibration and stray light

The implementation of the 'star sense' and 'horizon sense' combination may suffer from significant misalignment hurdles that impact on accuracy. The intention is that both sensors will be calibrated prior to launch. However, it is well known that during launch and operations, a number of external factors will influence the mechanical alignment between the sensors.

This challenge will be overcome by utilising unbiased star measurements through both sensors. 'Horizon sense' may also act as a star tracker, detecting stars instead of identifying the horizon edge. So, by calculating the inertial attitude for both cameras, labelled A and B, the interlock matrix might be calculated by,

$$T_{AB} = T_{IA}^{-1} T_{IB}. \quad (12)$$

This term may then be introduced into Eq. (7) as an additional matrix multiplication.

For the CROSS optical navigation assembly, the expected perfor-mance of this misalignment calibration through one observation is approximately 10" [43]. This accuracy should improve over a contin-uous set of observations.

Misalignment calibration would operate best during eclipse when the Earth illumination is at its lowest point. However, during daytime, the thermal fluctuations on board the satellite are expected to be significant enough for the structural expansion and contraction to impair the misalignment. The question is then if misalignment calibration can be performed during daytime to compensate.

Stray light modelling is complex to model, but simplifications might be made to provide an approximation to the extent of camera saturation. The irradiance of in-field stray light can be modelled by,

$$E_{ifsl} = E_{earth} BSDF\left(\frac{r}{2L}\right), \quad (13)$$

where E_{earth} is the radiance from an illuminated Earth, approximated to 14 W/m^2, r is the distance from the illumination source and L is the pixel distance of the sensor. The Bi-directional Scattering Distribution Function (BSDF) models the scattering of light through material interactions. For a glass lens, this can be written as,

$$BSDF\left(\frac{r}{2L}\right) = b_0 \left[1 + \left(\frac{r}{2Ll}\right)^2\right]^{-C/2}, \quad (14)$$

where,

$$b_0 = \frac{2\pi \Delta n^2 B^2}{\lambda^4} \frac{R_q^2(-C - 2)}{1 - \left(1 + \frac{B^2}{\lambda^2}\right)^{(C+2)/2}}, \quad (15)$$

$l = \frac{\lambda}{B}$, λ is the light wavelength, Δn is the refractive index difference between the two medium (which for glass in a vacuum is 1.52), R_q is the surface roughness constant (which for a glass lens might be approximated to 10 Å), and B and C are a set of modelling constants usually set to $B = 200(10^{-6})$ and $C = 1.55$ [52].

A model of a star map and Earth might then be simulated, with the Earth placed in the image corner. The stars irradiance is dependent on the apparent magnitude m, star temperature T and wavelength, written as [53],

$$E_{star} = \frac{L_o 10^{0.4(M_o - m)}}{400\pi\beta^2 \sigma T^4} \frac{2\pi c}{\lambda^4 (e^{hc/\lambda kT} - 1)}, \quad (16)$$

where L_o and M_o are the absolute brightness and magnitude of the Sun, β is the conversion factor from parsec to metres, σ, h and k are the Stefan, Planck and Boltzmann constants respectively, and c is the speed of light.

A simulated star map and Earth are illustrated in Fig. 5 using the simulated parameter approach just described. This simulation also successfully identified stars. Using the procedure outlined in Section 2.2.1 for attitude.

Determination from a typical star tracker, the accuracy delivered is 30".

When introduced to the misalignment correction, this delivers a combined offset of approximately 0.01°. This misalignment is intro-duced to the full simulation, which is presented as part of Section 3.4.
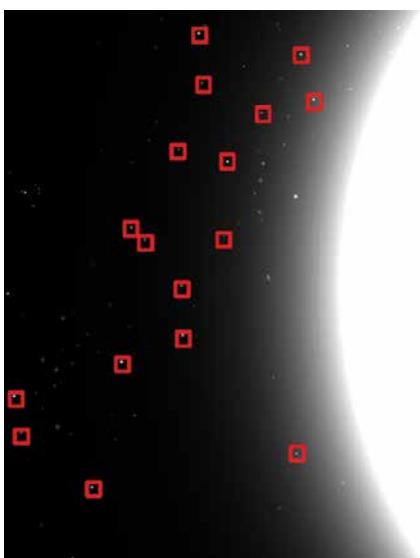

Fig. 5. Simulated star and Earth image with a successfully identified star map with a spacecraft at 450 km altitude above surface.

3.3.2. Atmospheric offset

The atmospheric offset is one of the key challenges for a LEO horizon estimate, or indeed for any planet with an atmosphere. This problem has not been given much study in the literature, with the most recent work by Christian [21].

Christian poses a solution by studying the potential illumination measured by the camera. He calculated an offset of the order of 25 km. However, this is distinctly during daylight operation, and will change during sunset/sunrise and eclipse. It is also dependent on the camera exposure time.

This estimate might be used as an initial estimate to the atmospheric offset. However, the estimate should be validated by use in a least squares filter. The known ellipsoidal parameters of the Earth and the orbit propagation model should provide sufficient information to further refine the horizon estimate.

The atmospheric offset ρ, assuming this is constant to all observed directions of the ellipsoid, may be incorporated in a modified ellipsoidal body matrix,

$$\widetilde{A} = \begin{bmatrix} \frac{1}{(a+\rho)^2} & 0 & 0 \\ 0 & \frac{1}{(b+\rho)^2} & 0 \\ 0 & 0 & \frac{1}{(c+\rho)^2} \end{bmatrix}. \quad (17)$$

The atmospheric offset might then be introduced as a state parameter estimate in the Kalman filter, modifying the state vector estimate in Eq. (8) to become,

$$x = \{r^T \quad v^T \quad \rho\}^T. \quad (18)$$

The EKF parameters are then calculated by the Jacobian. There is no dependence to the atmospheric offset in the orbit propagation.

The atmospheric offset can be reset throughout orbit as the illumination changes from day to night, where the boundary height seen in the image plane ρ raises and lowers.

3.4. Expected performance

The methodology presented in this section are now simulated and compared. They are generated from a scenario of lost-in-space, where no prior position is known by the user. This is a worst case scenario. Horizon points are varied with a 2 px error, as identified in Section 2.2.2, and the 'star sense' and 'horizon sense' cameras are simulated according to specifications contained within Table 2.

The simulation is run for nearly two orbits. An atmospheric offset ρ is set to 25 km [21], with an initial estimate error at 1 km. The entire filter is run over two orbital periods. The simulation is run on MATLAB.

Given the models seek to aid LEO satellites, orbital altitudes at 300 km, 600 km and 1200 km are compared in Fig. 6. The accuracy and precision (standard deviation) is reported in Table 3. Each result is given by an error and standard deviation for cross-track, along-track and radial error terms.

A steady state is achieved in Fig. 6 after a single orbit, which for a LEO satellite is approximately 90 min. Each of the parameters presented in Table 3 is calculated after the first orbit of 90 min, where it is assumed the solution has converged. The margin of error below 100 m satisfies requirements for some LEO applications reported in Table 1. There ap-pears to be no strong dependence on orbital height at close proximity to the body. The estimated standard deviation indicates strong stability after the solution has converged.

To explore the atmospheric offset correction, the estimated ρ values over the simulation are presented in Fig. 7. The reduction of error is fast, with no noticeable impact to the simulation accuracy. The offset is fast reduced to an approximate 10 m average within 10 min. The standard deviation of the error is also included as a dashed line in this plot.

4. Introduction to navigation infrastructure

As raised in the introduction to this work, not only may visual-based PNT be utilised by spacecraft in-orbit but also as a supporting system for terrestrial and lunar ranging services. Recent plans for LEO mega- constellations [23,24], as well as lunar orbit [25,26,38], envisage the delivery of a new-type of ranging signal. This would be unlike traditional ranging like GPS and Galileo, where the signals are distributed freely, but instead be closed and protected.

Present infrastructure only considers the source of orbit determina-tion to be derived by GNSS or ground infrastructure. Given the restricted availability of tracking stations across the globe, GNSS is even being solely relied upon for the generation of ephemeris on-board the satellites. However, these systems may not be treated as a back-up, as they would then be unable to operate if GNSS is denied or unavailable [28]. Thus, a an alternative to GNSS and RF-derived orbit determination should be considered, like the visual-based system treated in this article.

The performance of a ranging service is dependent on the signal-in- space accuracy, which refers to the accuracy of the delivered ranging signal, and the satellite geometry, quantified by the Geometric Dilution of Precision (GDOP). The signal-in-space performance is a combination of error terms from the atmospheric delay σ_{atm}, receiver σ_{rcv} and satellite noise σ_{sat}, timing σ_{clock} and orbit determination σ_{eph}. These terms are combined by,

$$\sigma_{URE}^2 = \sigma_{eph}^2 + \sigma_{clock}^2 + \sigma_{atm}^2 + \sigma_{rcv}^2 + \sigma_{sat}^2 + \sigma_{other}^2, \quad (19)$$

where σ_{other} incorporates all other terms. For proposed LEO infrastructure, these factors are on the order of magnitude 0.1–1 m [24], except for the ephemeris term, which if not relying on GNSS might be greater.

It should be mentioned that what is being proposed is not a replacement but a supporting system to assure that a ranging service may still be delivered in the absence of GNSS. As discussed in Section 2, this is a requirement for both maritime and aviation applications to treat the system as an alternative or back-up. This is also required for a ranging service beyond Earth and on the Moon, as GNSS coverage is very limited.

In Section 3.4, the performance of visual-based PNT for orbit determination was recorded for radial, along- and cross-track. This may be transformed into an equivalent ephemeris error by using the work of Chen in Ref. [54]. The principles are now introduced but only a limited discussion.

Chen considers the probability distribution of ranging signals distributed across the user plane on Earth by a single satellite. The unit vectors of pointing to positions

on the surface are described by elevation α and azimuth β angles for a satellite at height h above the surface as,

$$l = \frac{1}{\sqrt{R_e^2 - 2R_e h \cos \alpha + h^2}} \begin{Bmatrix} R_e \sin \alpha \cos \beta \\ R_e \sin \alpha \sin \beta \\ R_e \cos \alpha - h \end{Bmatrix}. \quad (20)$$
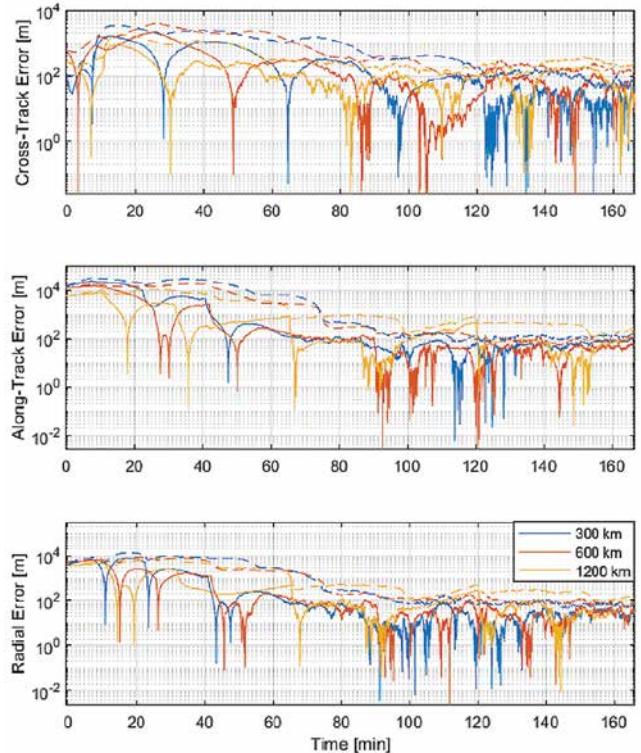
Fig. 6. Position performance for different orbit altitudes above the Earth's surface. The dashed line represents the 3σ standard deviation of the filtered solutions.

Table 3: Performance for Radial, Cross- and Along-track measurements for varying altitudes.

Altitude	Accuracy (Precision)		
	Cross	Along	Radial
300 km	0.62 m (39.1 m)	0.14 m (65.9 m)	−12.6 m (25.0 m)
600 km	−19.18 m (41.3 m)	−32.54 m (43.5 m)	−16.2 m (31.0 m)
1200 km	2.83 m (31.0 m)	68.4 m (99.9 m)	−51.4 m (61.2 m)
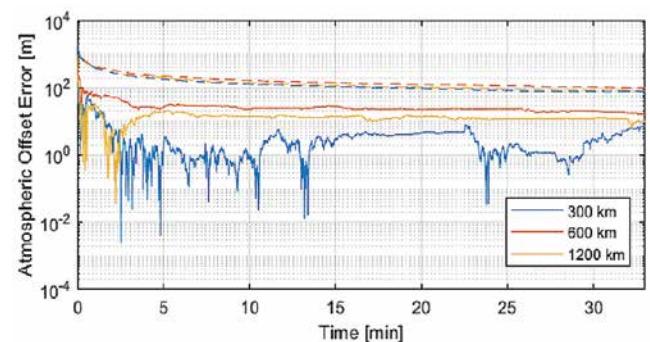
Fig. 7. Atmospheric offset performance for different orbit altitudes above the Earth's surface. The dashed line represents the 3σ standard deviation of the filtered solutions.

The probability of satellite coverage across this surface of the Earth is then,

$$p(\alpha, \beta) = \frac{\sin \alpha d\alpha d\beta}{2\pi(1 - \sin \theta)}, \qquad (21)$$

where θ is the angle of surface coverage from the zenith to the horizon. Calculating across the variable range of angles $p(\alpha, \beta) = \frac{\sin \alpha d\alpha d\beta}{2\pi(1 - \sin \theta)}$, and $\beta \in [0, 2\pi]$, the root-mean-square formula for the ephemeris is,

$$\sigma_{eph}^2 = \int_0^{2\pi} \int_0^{\frac{\pi}{2}-\theta} \frac{o^T l^2 \sin \alpha d\alpha d\beta}{2\pi(1 - \sin \theta)}, \qquad (22)$$

where $o = \{-C, A, -R\}$ for the cross-track C, along-track A and radial R errors.

Considering the orbit determination errors reported in Table 3, the equivalent error for the ephemeris σ_{eph} is approximately 50 m across orbital altitudes 300–1200 km.

The user error in three-dimensions is calculated by a combination of the GDOP and user range error. This is simply computed by,

$$\sigma_{3D} = \text{GDOP} \bullet \sigma_{URE}. \qquad (23)$$

The GDOP has been reported across MEO GNSS and LEO mega constellations in the pioneering work of Reid et al. [23] that summarises the GDOP expected across each varying orbital geometry.

Upcoming LEO constellations include Teledesic, OneWeb and Star-link. According to Fig. 8, the expected GDOP is on the order of 1.0. Substituting this into (23) using the expected error of
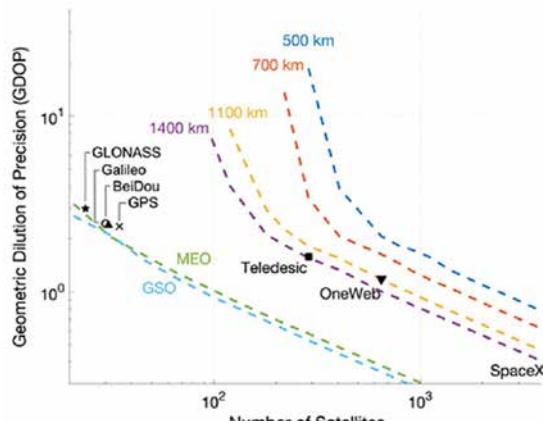
Fig. 8. Comparison of user GDOP (95th percentile) as a function of constellation size and altitude for a 5 deg elevation mask [23].

50 m for the user range error σ_{URE}, the potential performance for a user position derived by such a ranging signal is 50 m.

Recalling the performances expected for aviation and maritime sectors, this result is promising to be applied across application domain where a back-up system would need to deliver a performance at 100 m. Thus, a vision-based orbit determination may be considered as an alternative technology to RF-based GNSS and ground station tracking for future LEO-based ranging systems. This could also be translated for use in a lunar positioning service, adopting a similar analysis.

5. Conclusions

The work introduces a visual-based PNT system and demonstrates this it is an alternative to GNSS and RF-derived positioning. This system is treated in the framework of being an orbit determination alternative for LEO satellites as well as being a supporting system to new concepts of GNSS in LEO and Lunar environments.

The potential performance delivered by such a system is better than 100 m. This is shown by simulating the orbit of a LEO satellite across multiple altitudes and calculating the standard deviation across along- track, cross-track and radial dimensions. Challenges for LEO operations are also considered, including eclipse and daytime operations as well as atmospheric bias in the observed horizon.

A visual-based PNT system might also be implemented as a form of orbit determination for proposed LEO ranging constellations. It was demonstrated that this can satisfy the requirements of most terrestrial user domains, including maritime and aviation. The results might also be treated in terms of lunar users as part of a lunar navigation service.

Declaration of competing interest

Acknowledgements

References

[1] B.A. Lampkin, D.W. Smith, A Hand-Held Sextant Qualified for Space Flight, NASA, Washington, DC, 1968.

[2] H.A. Garcia, W.J. Owen, Design and analysis of a space sextant for high altitude navigation, J. Spacecr. 13 (12) (May 1975) 705–709, https://doi.org/10.2514/ 3.57131.

[3] B.A. Lampkin, Sextant sighting performance for space navigation using simulated and real celestial targets, Navigation 12 (4) (1965) 312–320, https://doi.org/ 10.1002/ J.2161-4296.1965.TB02149.X.

[4] J.D. Vedder, Star trackers, star catalogs, and attitude determination - probabilistic aspects of system design, J. Guid. Control Dynam. 16 (3) (1993) 498–504, https:// doi.org/10.2514/3.21037.

[5] C.C. Liebe, Accuracy performance of star trackers - a tutorial, IEEE Trans. Aero. Electron. Syst. 38 (2) (2002) 587–599, https://doi.org/10.1109/ TAES.2002.1008988.

[6] T. Dzamba, J. Enright, Optical Trades for Evolving a Small Arcsecond Star Tracker, IEEE Aerospace Conference, 2013, https://doi.org/10.1109/AERO.2013.6497172.

[7] J. Critchley-Marrows, X. Wu, I. Cairns, Stellar navigation on the Moon - a compliment, support and back-up to lunar navigation, in: Proceeding of the ION ITM 2022, 2022, pp. 616–631. Long Beach, CA.

[8] D. Mortari, C. D'Souza, R. Zanetti, Image processing of illuminated ellipsoid, J. Spacecr. Robot. 53 (3) (2016) 448–456, https://doi.org/10.2514/1.A33342.

[9] J.A. Christian, A tutorial on horizon-based optical navigation and attitude determination with space imaging systems, IEEE Access 9 (2021) 19819–19853, https://doi.org/10.1109/ACCESS.2021.3051914.

[10] C.T.F. Kühl, Combined Earth/ Star Sensor for Attitude and Orbit Determination of Geostationary Satellites, University of Stuttgart, Stuttgart, 2005.

[11] J.A. Christian, S.B. Robinson, 'Noniterative Horizon-Based Optical Navigation by Cholesky Factorization' 39 (12) (2016) 2755–2763, https://doi.org/10.2514/1. G000539.

[12] V.H. Adams, M.A. Peck, Interplanetary optical navigation, in: AIAA Guidance, Navigation, and Control Conference, Reston, Virginia, 2016, https://doi.org/ 10.2514/6.2016-2093.

[13] Y. Dachev, A. Panov, 21st century Celestial navigation systems, in: Proceedings of the 18th Annual General Assembly AGA, Varna, Bulgaria, 2017, pp. 1–9 [Online]. Available: https://www.researchgate.net/publication/341479107_21_st_century_ Celestial_navigation_systems.

[14] N. Ogawa, et al., Image-based autonomous navigation of Hayabusa2 using artificial landmarks: design and in-flight results in landing operations on asteroid ryugu, in: AIAA Scitech 2020 Forum, American Institute of Aeronautics and Astronautics, 2020, https://doi.org/10.2514/6.2020-0225.

[15] M. Pugliatti, V. Franzese, P. Panicucci, F. Topputo, TINYV3RSE: the DART vision- based navigation test-bench, in: AIAA SCITECH, American Institute of Aeronautics and Astronautics, 2022, https://doi.org/10.2514/6.2022-1193.

[16] D.A. Lorenz, et al., Lessons Learned from OSIRIS-REx Autonomous Navigation Using Natural Feature Tracking, IEEE Aerospace Conference, 2017, pp. 1–12, https://doi.org/10.1109/AERO.2017.7943684.

[17] T. Qin, D. Qiao, M. Macdonald, Relative orbit determination for unconnected spacecraft within a constellation, J. Guid. Control Dynam. 44 (3) (2021) 614–621, https://doi.org/10.2514/1.G005424.

[18] J.A. Christian, 'Accurate Planetary Limb Localization for Image-Based Spacecraft Navigation' 54 (3) (2017) 708–730, https://doi.org/10.2514/1.A33692.

[19] D. Mortari, F. de Dilectis, R. Zanetti, Position estimation using the image derivative, Aerospace 2 (2015) 435–460, https://doi.org/10.3390/ AEROSPACE2030435.

[20] J. Critchley-Marrows, D. Mortari, Vision-based navigation in low Earth orbit – using the stars and horizon as an alternative PNT, Adv. Space Res., Jan. (2023), https://doi.org/10.1016/j.asr.2023.01.047.

[21] J.A. Christian, Horizon-based optical navigation using images of a planet with an atmosphere, AIAAAAS Astrodyn. Spec. Conf. 2016 (2016), https://doi.org/ 10.2514/6.2016-5442.

[22] J.A. Christian, L. Benhacine, J. Hikes, C. D'Souza, Geometric calibration of the orion optical navigation camera using star field images, J. Astronaut. Sci. 63 (4) (2016) 335–353, https://doi.org/10.1007/s40295-016-0091-3.

[23] T.G.R. Reid, A.M. Neish, T. Walter, P.K. Enge, Broadband LEO constellations for navigation, Navigation 65 (2) (Jun. 2018) 205–220, https://doi.org/10.1002/ NAVI.234.

[24] P.A. Iannucci, T.E. Humphreys, Fused Low-Earth-Orbit GNSS, Sep. 2020. Accessed: Aug. 13, 2022. [Online]. Available: http://arxiv.org/abs/2009.12334.

[25] P. Giordano, et al., Moonlight navigation service - how to land on peaks of eternal light, in: Proceedings of the 72nd International Astronautical Congress, 2021, pp. 1–14. Dubai.

[26] P. Giordano, F. Malman, R. Swinden, P. Zoccarato, J. Ventura-Traveset, The lunar pathfinder PNT experiment and Moonlight navigation service: the future of lunar position, navigation and timing, Proc. 2022 Int. Tech. Meet. Inst. Navig. (Jan. 2022) 632–642, https://doi.org/10.33012/2022.18225.

[27] M. Schonfeldt, et al., A system study about a lunar navigation satellite transmitter system, Eur. Navig. Conf. ENC 2020 (2020), https://doi.org/10.23919/ ENC48637.2020.9317521.

[28] A.J. Owens, T. Richardson, J. Critchley-Marrows, The Feasibility of a VDE-SAT Ranging Service as an Augmentation to GNSS for Maritime Applications, Oct. 2021, pp. 591–616, https://doi.org/10.33012/2021.18150.

[29] 'ICAO Doc, AN10-1 - Annex 10 (Aeronautical Telecommunications) to the Convention on International Civil Aviation, Volume I - Radio Navigation Aids, International Standards and Recommended Practices (SARPs)', International Civil Aviation Organisation, 2006.

[30] P. Williams, 'MarRINav - Maritime Context and Requirements', General Lighthouse Authority, Harwich, Aug. 2019.

[31] Satellite-derived Time and Position: A Study of Critical Dependencies, Government Office for Science, London, Jan. 2018.

[32] EUSPA EO and GNSS Market Report, EUSPA, Prague, 2022.

[33] Global Navigation Satellite System (GNSS) Manual, International Civil Aviation Organisation, Quebec, 2005.

[34] R-129 GNSS Vulneraibility and Mitigation Measures, International Association of Lighthouse Authorities, Dec. 2012.

[35] D.G. Muff, Orbit determination requirements for synthetic aperture radar, Int. Geosci. Remote Sens. Symp. IGARSS 2 (1998) 697–700, https://doi.org/10.1109/ IGARSS.1998.699554.

[36] W.J. Larson, J. Richard Wertz, Space Mission Analysis and Design, Microcosm, 1992. Accessed: Aug. 13, 2022. [Online]. Available: https://link.springer.com /book/9780792319986.

[37] B. Coffee, R. Bishop, K. Cahoy, Propagation of CubeSats in LEO using NORAD two line element sets: accuracy and update frequency, in: AIAA Guidance, Navigation, and Control (GNC) Conference, American Institute of Aeronautics and Astronautics, 2013, https://doi.org/10.2514/6.2013-4944.

[38] LunaNet Concept of Operations and Architecture, NASA, Sep. 2020.

[39] 'Above Us Only Stars — C4ADS', Centre for Advanced Defence, Studies [Online]. Available: https://www.c4reports.org/aboveusonlystars, 2019.

[40] M. Harris, Ghost ships, crop circles, and soft gold: a GPS mystery in Shanghai, MIT Technology Review (2019) [Online]. Available: https://www.technologyreview. com/2019/11/15/131940/ ghost-ships-crop-circles-and-soft-gold-a-gps-mystery- in-shanghai/.

[41] D. Goward, GPS disrupted for maritime in Mediterranean : GPS World, Nov [Online] Available: GPS World (2018) https://www.gpsworld.com/gps-disrupted -for-maritime-in-mediterranean-red-sea/.

[42] 'ESA Moonlight Initiative, LCNS User Scenario Document', European Space Agency, Noordwijk, Nov, 2020.

[43] M. Suntup, et al., Implementation of a WFOV star tracker in CubeSat and small satellite attitude determination systems, Proceedings of the 43rd COSPAR Scientific Assembly, Sydney, Feb 43 (2021) 59. Accessed: Aug. 25, 2022. [Online]. Available: https://ui.adsabs.harvard.edu/ abs/2021cosp...43E..59S/abstract.

[44] J. Critchley-Marrows, X. Wu, Investigation into integrated attitude determination in high-precision CubeSats, in: Proceedings of the 68th International Astronautical Congress, Sep. 2017. Adelaide.

[45] J. Critchley-Marrows, X. Wu, Investigation into star tracker algorithms using smartphones with application to high-precision pointing CubeSats, Trans. Jpn. Soc. Aeronaut. Space Sci. 17 (3) (2019) 327–332, https://doi.org/10.2322/ TASTJ.17.327.

[46] J. Brown, K. Stubis, K. Cahoy, TETRA: star identification with hash tables, Logan, UT, in: 31st Annual AIAA/ USU Conference on Small Satellites, Aug. 2017, pp. 1–12. . [Online]. Available: https://github.com/brownj4/Tetra.

[47] F.L. Markley, J.L. Crassidis, Filtering for attitude estimation and calibration, in: Fundamentals of Spacecraft Attitude Determination and Control, Springer Science and Business Media, New York, 2014, pp. 235–343.

[48] A. Fitzgibbon, M. Pilu, R.B. Fisher, Direct least square fitting of ellipses, IEEE Trans. Pattern Anal. Mach. Intell. 21 (5) (1999) 476–480, https://doi.org/ 10.1109/34.765658.

[49] M.A. Fischler, R.C. Bolles, Random sample consensus, Commun. ACM 24 (6) (1981) 381–395, https://doi.org/10.1145/358669.358692.

[50] M. Garcia, International Space Station Multimedia, 2013. NASA, Jun. 20, http ://www.nasa.gov/mission_pages/station/multimedia/index.html. (Accessed 12 June 2022). accessed.

[51] J.A. Christian, Optical navigation using planet's centroid and apparent diameter in image, J. Guid. Control Dynam. 38 (2) (Feb. 2015) 192–204, https://doi.org/ 10.2514/1.G000872/ASSET/ IMAGES/LARGE/FIGURE12.JPEG.

[52] E.C. Fest, Scattering from optical surface roughness and coatings, Stray Light Analysis and Control 1 (2013) 61–76, https://doi.org/10.1117/3.1000980.

[53] E. Tola, Black-body SNR formulation of astronomical camera systems, IEEE Sensor. J. 15 (9) (2015), https://doi.org/10.1109/JSEN.2015.2427911.

[54] L. Chen, et al., Study on signal-in-space errors calculation method and statistical characterization of BeiDou navigation satellite system, Lect. Notes Electr. Eng. 243 (2013) 423–434, https://doi.org/10.1007/978-3-642-37398-5_39.

Abbreviations

EKF, Extended Kalman Filter; GDOP, Geometric Dilution of Precision; GNSS, Global Navigation Satellite System; LCNS, Lunar Communication and Navigation Satellites; LEO, Low Earth Orbit; MEO, Medium Earth Orbit; PNT, Position Navigation and Timing; RF, Radio Frequency; SAR, Synthetic Aperture Radar.

IBM and NASA Open Source Largest Geospatial AI Foundation Model

IBM and open-source AI platform Hugging Face has announced that IBM's watsonx.ai geospatial foundation model – built from NASA's satellite data – will be available on Hugging Face. It will be the largest geospatial foundation model and the first-ever open-source AI foundation model built in collaboration with NASA.

As part of a Space Act Agreement with NASA, IBM set out earlier this year to build an AI foundation model for geospatial data. And now, by making a geospatial foundation model available, efforts can advance to democratize access and application of AI to generate new innovations in climate and Earth science.

The model – trained jointly by IBM and NASA on Harmonized Landsat Sentinel-2 satellite data (HLS) over one year across the continental United States and fine-tuned on labeled data for flood and burn scar mapping — has demonstrated to date a 15 percent improvement over state-of-the-art techniques using half as much labeled data. With additional fine tuning, the base model can be redeployed for tasks like tracking deforestation, predicting crop yields, or detecting and monitoring greenhouse gasses. *https://newsroom.ibm.com*

Overture Maps Foundation releases first world-wide open map dataset

The Overture Maps Foundation (OMF), a collaborative effort to enable current and next-generation interoperable open map products, announced the release of its first open map dataset.

It includes four unique data layers: Places of Interest (POIs), Buildings, Transportation Network, and Administrative Boundaries. These layers, which combine various sources of open map data, have been validated and conflated through a series of quality checks, and are released in the Overture Maps data schema which was released publicly in June 2023.

The Places dataset includes data on over 59 million places worldwide and will be a foundational element of navigation, local search and many other location-based applications. *https://overturemaps.org*

Mapbox 3D mapping designed to enhance location awareness

Mapbox has released new platform updates to enhance user's 3D mapping experience by adding powerful dynamic lighting capabilities and landmark 3D buildings. The new ready-to-use platform aims to enhance wayfinding and spatial orientation for users and provides a polished canvas for custom location data. *www.mapbox.com*

RAK to implement 'Parcel Fabric' technology for managing spatial data

Ras Al Khaimah (RAK) has become the first city in the Middle East to implement "Parcel Fabric" technology for managing spatial land data, based on a certificate granted by the Esri.

In partnership with the GIS Centre, Ras Al Khaimah Municipality is using the Parcel Fabric technology to manage the spatial information of land plots through the rules and definitions it defines. This spatial data forms the basis of the systems that register land ownership and other real estate interests and is, therefore, key to the effective management of any city. Adopting the technology, which is linked to the land registry, will help preserve the rights of owners and property investors in the Emirate. The system improves records' accuracy, increasing operations efficiency and reducing the time required for tasks such as modifying and updating land records.

Parcel Fabric allows cadastral data to be fit for purpose by storing the required metrics and metadata, such as the method of capture, date, spatial accuracy and historical lineage, for use and publishing as needed. In addition, the built-in data quality management mechanisms ensure the accuracy of other key elements, such as topology and plot attribution. *www.zawya.com* ⌐

NASA to acquire Synthetic Aperture Radar Data from ICEYE

ICEYE US has won a contract under a Blanket Purchase Agreement (BPA) with NASA announced earlier this year. The contract enables NASA to acquire ICEYE's synthetic-aperture radar (SAR) data for evaluation by scientific and academic communities to determine suitability for advancing NASA's Earth Science research objectives. The BPA is funded by the Earth Science Division of the Science Mission Directorate. *www.nasa.gov*

Viasat opens real-time earth ground station in Japan

Viasat announced the opening of a Real-Time Earth (RTE) ground station in Hokkaido, Japan enabling its customers the ability to downlink Ka-band payload data in the northwestern Pacific at the site hosted by its partner Infostellar

Viasat is establishing itself as a global leader in Ka-band support for low earth orbit (LEO) missions with its ability to downlink Ka-band payload data with a 7.3m full motion antenna at the Hokkaido site and is postured to support current and future government and commercial satellite programs. *https://news.viasat.com*

Goa govt to rope in satellite imagery firm to map out CRZ violations

The state government of Goa, India will engage a company with expertise in satellite imagery to map structures that existed on the state's shoreline before 1991 to understand the extent of the Coastal Regulation Zone (CRZ) violations.

The Goa State Coastal Zone Management Authority (GSCZMA) had issued show cause notices to 275 structures, giving them time to respond with documentation to prove that they existed before 1991. The notices were issued after the October 2022 order of the High Court against the gross violations in CRZ areas, the senior GSCZMA official said. ⌐

TIER IV and Axell unveil Autoware Accelerator prototypes

TIER IV has successfully partnered with Axell Corporation, a Japan-based computer hardware company, to conduct a collaborative research project aimed at creating a new application-specific system-on-chip (SoC) and software platform for autonomous vehicles. The project culminated in a demonstration, showcasing the power and performance advantages of the Autoware Accelerators. These hardware accelerators are custom-designed specifically for the Autoware architecture. These collaborative research efforts were funded by the "Innovative AI Chip and Next-Generation Computing Technology Development" project, sponsored by the New Energy and Industrial Technology Development Organization (NEDO). *https://tier4.jp/en*

Autonomous vehicle lidar integration with NVIDIA DRIVE and Omniverse

Hesai Technology announced a collaboration with NVIDIA to integrate Hesai's cutting-edge lidar sensors within the NVIDIA DRIVE and NVIDIA Omniverse ecosystems. NVIDIA DriveWorks is the foundation for autonomous vehicle software development and a trusted solution for creating and deploying autonomous driving applications. Developers building on DriveWorks will be able to effectively integrate Hesai's lidar sensors into their vehicles, leading to more efficient and reliable autonomous driving systems. *www.hesaitech.com*

RapidDeploy launches a new mobile app for first responders

RapidDeploy, a cloud-native solution provider for Public Safety, announced Lightning, a new mobile app that delivers 911 call data and critical information directly to first responders' mobile devices, including smartphones and tablets. Kansas in the USA will be the first statewide customer to harness the power of Lightning, enabling the sharing of data across state and local stakeholders, and providing more than 100 911 centers and 24,000 first responders access to real-time, life-saving information to aid in response efforts.

First responders leveraging the mobile app will have access to real-time 911 call data, location accuracy, video feeds, GIS mapping layers, and more, providing situational awareness, improving joint inter-agency communications, and delivering a new level of visibility amongst responders. *https://rapiddeploy.com* ⬐

New Galileo station goes on duty

Galileo's ground segment has gained a new asset, the Telemetry, Tracking and Control (TT&C) facility — a 13.5-m parabola dish mounted on top of a 10-m high building structure of made of steel and concrete. It is based within Europe's launch site in Kourou, French Guiana, beside TTCF-2.

The TT&C antennas are uncrewed and operate on a fully automated basis from the two Galileo control centers located in Oberpfaffenhofen, Germany, and Fucino, Italy. The TT&C antennas are crucial to regular communication with the Galileo satellites.

This latest antenna will play an important role during the upcoming modernization activities of the earlier TT&C antennas in the station network, which have been in service for several years. TTCF-7 will take over their tasks during the maintenance activities when they need to be taken offline. *www.esa.int*

Thales partners with ESA on Galileo cybersecurity and enhancements

As part of G2G IOV SECMON, Thales is leading the consortium, including the Italian group Leonardo, to expand the scope of security monitoring and include the new assets in the G2G system. It will also introduce automated incident response and network traffic monitoring. In addition, the solution will be capable of storing significant amounts of incident response data. To meet this challenge, Thales will deliver a solution built on a scalable, flexible architecture derived from its Cybels range of security supervision products and incorporating big data capabilities.

A cybersecurity contract for better protection from quantum threats New threats from quantum computers capable of breaking existing cryptographic algorithms have the potential to compromise long-term data security. Thales has been tasked by ESA within the consortium it leads to draw on its world-renowned cryptography expertise. *www.thalesgroup.com*

GNSS signals monitor volcano activity in Japan

The Japan Meteorological Agency (JMA) has reported that on July 10-17, data from GNSS signals indicated continuing minor inflation at shallow depths beneath Mount Ioyama, located on the northwest flank of the Karakuni-dake stratovolcano in the Kirishimayama volcano group in Japan.

Shallow volcanic earthquakes were recorded and vigorous fumarolic activity was visible at the fumarolic on the south side of Mount Ioyama. The alert level remained at two, on a five-level scale, and the public was warned to stay 1 km away from Mount Ioyama.

Indonesia, Japan explore cooperation to develop satellite navigation

Indonesia's National Research and Innovation Agency (BRIN) and Japan's National Space Policy Secretariat of the Cabinet Office have signed a letter of intent (LOI) for cooperation to develop and utilize satellite navigation systems and technologies.

BRIN's Deputy of Research and Utilization of Innovation, R. Hendrian, stated that satellites and their technologies are crucial for archipelagic states like Indonesia. In terms of cooperation with Japan, BRIN's Head of Research Organization for Electronics and Informatics, Budi Prawara, mentioned that Japan's Quasi-Zenith Satellite System (QZSS) could be utilized. *https://isp.page* ⬐

PNT solution with 5G and LTE signals

NextNav has has successfully tested its positioning and timing solution that combines the company's assured PNT TerraPoiNT system with existing LTE and 5G network signals. The test, which took place in and around San Jose, California, demonstrates how TerraPoiNT signals can be integrated with existing cellular signals to deliver accurate 3D positioning and timing information that is not reliant on conventional satellite-based GPS and GNSS signals. *nextnav.com*

ProStar, Leica Geosystems announce technology integration

ProStar Holdings has announced a technology integration with Leica Geosystems, which combines ProStar's utility mapping software, PointMan, and Leica Geosystems precision GPS/GNSS receivers for GIS asset data collection. The technology integration provides a precise and comprehensive data collection solution to capture, record, and display the precise location of critical underground infrastructure anywhere in the world with the Leica Geosystems receivers. *hexagon.com*

Xona accelerates commercial LEO GPS alternative

Xona Space Systems Inc has partnered with the Air Force Research Laboratory (AFRL) and the U.S. Space Force to work toward a secure Low Earth Orbit (LEO) PNT architecture leveraging Xona's PULSAR™ service. This $1.2M Direct to Phase II SBIR (D2P2) contract was awarded through an AFWERX SBIR Open Topic after Xona successfully demonstrated the capability of their patented LEO PNT architecture using the "Huginn" demo satellite in late 2022. *www.xonaspace.com*

Q–CTRL and Australia's Department of Defence partnership

Q-CTRL has partnered with Australia's Department of Defence to develop quantum sensors that will deliver quantum-assured navigation capability for military platforms.

The company's partnership is a multi-year effort to field-deploy and validate miniaturized systems on defense platforms. It represents one of the first international partnerships between government and the private sector to apply quantum technology in real defense settings. *https://q-ctrl.com*

ComNav device aids in skyscraper completion

Sweden's tallest building, Karlatornet, is expected to be completed in July, 2023. Karlatornet will be Gothenburg's first skyscraper with its 246 meters. It has 74 floors and covers an area of 143,000 square meters, this inspirational new tower will mark a shift from traditional development patterns in the country.1 It is worth mentioning that 4 x SinoGNSS T300 have been used as "Active Control GNSS Points" on the building top during the construction for delivering 3D coordinates for Total Stations. One SinoGNSS T300 has been used as Base Station. The Core Wall Control Survey is a method invented by Prof. Joël van Cranenbroeck the first time for the Burj Khalifa in Dubai. The PPK mode was used to derived the most accurate results. *www.comnavtech.com*

ModalAI launches the Starling

ModalAI, Inc has announced the availability of its drone - Starling. At only 275 grams and with an impressive 30+ minutes of flight time, it is ModalAI's lightest and longest flying development drone. With Blue UAS Framework 2.0 autopilot, VOXL 2, at its core, it accelerates the development of commercial drone solutions for OEMs looking to realize a breakthrough in autonomy across a diverse set of industries. *www.modalai.com*

DroneShield launches area–specific satellite denial systems

DroneShield Ltd. has launched an initial order from a defense customer for its target area-specific Satellite Denial Systems. Global Navigation Systems (GNSS) are used around the world, while the most well-known are GPS, GLONASS, Galileo and BeiDou systems.

DroneShield has used GNSS denial against drones and UAVs for a number of years as part of the smart defeat capability within its products. The company has developed a number of unique techniques.

A Five Eyes government has requested that DroneShield develop this capability a step further through a paid R&D project. This project is expected to follow up with a series of further projects, each project including more advanced development of the system. *www.droneshield.com*

Locana extends OpenStreetMap support

Locana is now a member of OpenStreetMap US, a nonprofit organization that helps support and grow the OpenStreetMap (OSM) project.

Conceived in 2004, OpenStreetMap is a free, open geographic database updated and maintained by a community of volunteers via collaboration. It broadens access to high-quality data, lowers the cost of harnessing location intelligence, and makes it possible for more organizations

SUBSCRIPTION FORM

YES! I want my |Coordinates

I would like to subscribe for (tick one)

☐ **1 year**
12 issues
Rs.1800/US$140

☐ **2 years**
24 issues
Rs.3400/US$200

☐ **3 years**
36 issues
Rs.4900/US$300

SUPER saver

*

First name ....

Last name ....

Designation ....

Organization ....

Address ....

....

City .... Pincode ....

State .... Country ....

Phone ....

Fax ....

Email ....

I enclose cheque no. ....

drawn on ....

date .... towards subscription

charges for Coordinates magazine

in favour of **'Coordinates Media Pvt. Ltd.'**

Sign .... Date ....

Mail this form with payment to:

Coordinates
A 002, Mansara Apartments
C 9, Vasundhara Enclave
Delhi 110 096, India.

If you'd like an invoice before sending your payment, you may either send us this completed subscription form or send us a request for an invoice at iwant@mycoordinates.org

* Postage and handling charges extra.

⬠ MARK YOUR CALENDAR

September 2023

Commercial UAV Expo
5-7, September 2023
Las Vegas, USA
www.expouav.com

ION GNSS+ 2023
11-15 September
Denver, Colorado, USA
www.ion.org

European Lidar Conference (ELC)
13 – 15 September
Cluj-Napoca, Romania
https://enviro.ubbcluj.ro

DroneX Trade Show & Conference 2023
26-27 September
London, United Kingdom
www.dronexpo.co.uk

October 2023

FIG COMMISSION 7 Annual Meeting 2023
2-4 October
The Netherlands
figcommission7@fig.net

Asian Conference on Remote Sensing (ACRS 2023)
30 October to 3 November
Taipei, Taiwan
https://acrs2023.tw

Intergeo 2023
10-12 October
Berlin, Germany
www.intergeo.de

November 2023

GEOINT Innovation Summit
1-2 November 2023
National Harbor, Maryland, USA
https://geoint.dsigroup.org

43rd INCA International Congress
06-08 November 2023,
Jodhpur, Rajasthan.
https://43inca.org

Trimble Dimensions 2023
6-8 November
Las Vegas, USA
www.trimble.com

GoGeomatics Expo
6-8 November 2023
Calgary, Canada
https://gogeomaticsexpo.com

The Smart GEO Expo 2023
8-10 November
Gyeonggi Province
Republic of Korea.
www.smartgeoexpo.kr/fairDash.do

18th International Conference on Location Based Services (LBS 2023)
20-22 November
Ghent, Belgium
https://lbs2023.lbsconference.org

The Pacific GIS and Remote Sensing Conference
27 November - 1 December
Suva, Fiji
https://pgrsc.org

---

to take advantage of insights from location data. *www.locana.co*

Namuga selects Lumotive to build next-gen 3D sensing solutions

Lumotive has entered into a commercial agreement with camera module specialist Namuga, which will leverage Lumotive's Light Control Metasurface (LCM) chipsets to develop solid-state lidar module solutions for a range of 3D sensing applications in the industrial, consumer and automotive markets.

Through this partnership, Namuga will leverage the LCM products to create a variety of next-generation solid state lidar modules that go beyond robotic automation solutions, extending into additional sectors like services, homecare, and logistics. *https://lumotive.com*

GeoCue unveils TrueView 3D Imaging Systems

GeoCue announces the release of three new, high-end TrueView 3D Imaging Systems. With unmatched precision and advanced capabilities, the all-new TV625, TV680, and TV680LR are set to redefine the standards of aerial imaging technology.
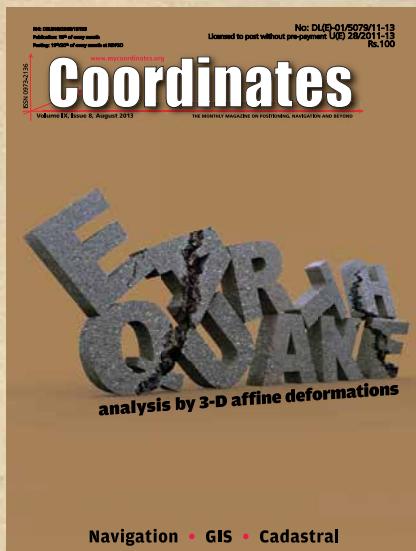
These three new systems, designed and manufactured in the USA, combine a very lightweight and compact laser scanner with 3 cameras to deliver unparalleled accuracy and efficiency in geospatial data collection. The new TV625, TV680, and TV680LR systems are NDAA compliant. *https://geocue.com*

Configurable GIS mobile app for surveying

1Spatial has launched the 1Capture, a customizable mobile application for data capture. It is a mobile GIS editing application that is multi-use and configurable. It provides accurate and reliable GIS data collection and editing in the field for a multitude of asset, job, and survey types. *https://1spatial.com* ⬠

In Coordinates

10 years before...

mycoordinates.org/vol-9-issue-8-August-2013

Earthquake analysis by 3-D affine deformations

James L Farrell
VIGIL Inc., Institute of Navigation Pacific PNT 2013, Honolulu Hawaii, USA

For investigation of earthquakes based on their affine degrees-of-freedom, methodology of another field –anatomy – is highly relevant. Instead of designated landmark sets coming from a group of patients, here they are associated with a series of days (e.g., from several days before to several days after a quake). Each landmark set is then subjected to a sequence of procedures thoroughly familiar to anatomy experts and succinctly reviewed herein.

Outdoor mobile field robot navigation

Chung-Liang Chang, Bo-Han Wu and Yong-Cheng Huang
National Pingtung University of Science and Technology, Taiwan, R.O.C.

This paper proposes a low-cost field robot capable of short-range field navigation, obstacle avoidance, color identification and spraying. Multiple micro-electro-mechanical sensors (MEMs) and multiple micro-controllers using a multi-layer fuzzy logic decision scheme were integrated to guarantee the autonomy of the mobile robot.

The Himalayan Tsunami in Uttarakhand

Anoop Nautiyal
Social and political commentator, former Chief Operating Officer, 108 Government emergency services, Uttarakhand

What should the leadership in Uttarakhand be doing right now? There are three things to focus on. Creating a vision, communicating that vision and executing the vision is what the leadership should concentrate on. Working on multiple fronts, the leader will have to inspire the millions of 'Uttarakhandis' and the rest of the nation who are all looking up to him for creating a holistic and consolidated strategic long-term rehabilitation and development plan for the State

Cadastral reform project in South Korea

Kang Sang-Gu, Kim Kyung-Il and Kim Tae-Hoon
Korea Cadastral Survey Corp., Seoul, Korea

The main purpose of this research is to propose the establishment of cadastral reference network based on the WGRS, and to make a fundamental plan which is unified into one national reference point

The use of GIS to forecast tourism demand

Dr Adnan AL-Jaber
Director of Geographical Information Systems MAS Center, Saudi Commission for Tourism and Antiquities, Kingdom of Saudi Arabia

This study showed that the full potential of the Huff model has not been recognized yet. Adding to the Huff model in the business analyst program in (ArcGIS), the package is a positive step in this direction. There are many applications for this model not only in the field of tourism demand, but in other tourism aspects.